CHALMERS
UNIVERSITY OF TECHNOLOGY

Causes of currents in the wind turbine bearings

Group 4 report for the design project

Babak AlikhanzadehAlamdari
Gokhan Tekin
Rogers Gatete Sengoga
Weijun Yuan

Report 2023:2

Department of Electrical Engineering
CHALMERS UNIVERSITY OF TECHNOLOGY
Gothenburg, Sweden 2017

Causes of currents in the wind turbine bearings

Babak AlikhanzadehAlamdari
Gokhan Tekin
Rogers Gatete Sengoga
Weijun Yuan

Technical report 2023:2
Department of Electrical Engineering
Division of Electric Power Engineering
CHALMERS UNIVERSITY OF TECHNOLOGY
SE-412 96 Gothenburg
Sweden, 2017

Causes of currents in the wind turbine bearings
Group 4 report for the design project
Babak AlikhanzadehAlamdari, Gokhan Tekin
Rogers Gatete Sengoga, Weijun Yuan
Department of Electrical Engineering
Chalmers University of Technology

Abstract

In some wind turbine nacelles, a current on the shaft is detected which can wear off the bearing gradually. The high maintenance cost is the main motivation of investigate the root cause of the current in the bearing. In the case of Big Gleen, the biggest wind turbine in Sweden, measurement is taken from eight critical points in the nacelle and Fast Fourier Transform(FFT) study on the data is carried out. Several possible root causes are proposed and the current in the shaft is studied by simulating the magnetic field around the shaft in COMSOL. In an opposite way, how much induced voltage to generate such amount of measurement current in the foot of the bearing is also simulated.

As for the measurement result, large amount of current is detected through the grounding cables which is highly suspicious. For the simulation result, based on specific assumptions, the possible root cause of the current is the induced voltage due to the power cables over the shaft. However, to verify the proposal of induced voltage, more accurate measurement equipment is needed for future work.

Keywords: Wind turbine, current, bearing, Fast Fourier Transform, COMSOL simulation, magnetic field.

Contents

1 Introduction **1**
- 1.1 Background . . . 1
- 1.2 Aim . . . 1
- 1.3 Scope . . . 2
- 1.4 Ethics . . . 2
- 1.5 Sustainability and Ethic Issue . . . 3

2 Theory **5**
- 2.1 Wind Turbine Electrical System . . . 5
  - 2.1.1 Perspective on some of electrical components in the wind turbine. . . . 5
  - 2.1.2 Power Cables . . . 6
  - 2.1.3 Magnetic field around current carrying conductors . . . 6
  - 2.1.4 Grounding System . . . 7
- 2.2 Magnetic Principles . . . 8
  - 2.2.1 Faraday's Law . . . 8
  - 2.2.2 Rogowski coil . . . 9
- 2.3 Mechanical Structure . . . 10
  - 2.3.1 Nacelle structure . . . 11
  - 2.3.2 The Bearings . . . 12

3 Methods **13**
- 3.1 Electrical Components and Circuit Diagram of the Nacelle . . . 13
- 3.2 Electrical Measurement Set-up . . . 14
- 3.3 Simulation . . . 18
  - 3.3.1 The geometry design . . . 18
  - 3.3.2 The Materials Selection . . . 19
  - 3.3.3 Simulation . . . 20
    - 3.3.3.1 Magnetic field study . . . 20
    - 3.3.3.2 Induced voltage determination . . . 21

4 Results and Analysis **23**
- 4.1 Measurements Results . . . 23
- 4.2 Simulation Results . . . 33
  - 4.2.1 Magnetic field study . . . 33
  - 4.2.2 Induced voltage determination . . . 35

5 Conclusion **37**
5.1 Results of Current Study 37
5.2 Future Work 38

Bibliography **39**

A Appendix 1 **I**
A.1 FFT Matlab codes I
A.2 The measurement data I

1

Introduction

1.1 Background

Wind is one of the renewable energy sources available today, it is the second largest renewable energy source in many countries including Sweden after hydro power. Wind offers many advantages compared to non-renewable sources of energy since it emits no pollution as fossil fuels do. This explains why it is one of the fastest-growing energy sources in the world.

However, the growth of wind energy extraction technology is facing serious challenges. One of the challenges is the current induced in the wind turbine bearings which leads to quick aging, high maintenance cost and replacement of bearings which largely affects the price of energy.

Basically, in a wind turbine like any other mechanical constructions with electrical machines, there can be a problem with electrical current through the mechanical roller bearing due to the presence of magnetic field associated to the presence of current.

The most unusual thing here is that the measurements in wind turbines have shown that in some cases there are currents in the bearings and other cases no current. It is therefore not obvious to explain why the current exists in some bearings and not others. The research has also shown that a bearing with a current will break in a shorter time compared with a bearing without a current.

In this report, the possible causes of current in the wind turbine bearings were proposed according to the data collected from Big Glenn in Göteborg, the biggest wind turbine in Sweden. Based on one of the hypothesis, simulations were conducted in COMSOL to verify the possible root cause.

1.2 Aim

The aim of this project is to propose some possible causes of the generation of the current on the bearing by the analysis on the data which is collected from Big Glenn. The simulation in COMSOL is used to verify one of the proposals.

1.3 Scope

In the aspect of data analysis, only the main electric components are considered. In other words, the auxiliary equipment is out of consideration. Also, the blades of the wind turbine are ignored since the current is believed to occur from the generator side. On the other side, the electric system is only considered before the transformer because the 10 kV cables are directly hung in the air in the tower rather than mounted in the nacelle.

In the simulation part since magnetic field around the power cable will be investigated in this project, the generator is neglected, and it is only considered as a voltage source. Besides, the electric circuit loop in this model is simplified only with bearing, shaft and nacelle ground. This assumption enables only the cable near the shaft to be focused. However, by doing this, some mechanisms such as PWM effect and coupling capacitors in the generator are missing. Even though they are ignored, since the problem is related to the voltage from generator side and the voltage source is implemented in the simulation, the model will be good enough to analyze causes of the current.

1.4 Ethics

In a workshop given by Stefan Lundberg, IEEE code of ethics have been introduced. According to IEEE, there are ten main code of ethics which can be considered in every project. Points chosen among those ten for our group are the third, the sixth and the eighth.

The third expression says "to be honest and realistic in stating claims or estimates based on available data" [1] which fits one of our project problems. In the simulation level, the generator and the converter side have been neglected for simplicity, however, it might affect the accuracy of the results since those parts are dynamic and the electric energy production and the transmission take place there.

The sixth code of ethics is included as "to maintain and improve our technical competence and to undertake technological tasks for others only if qualified by training or experience, or after full disclosure of pertinent limitations"[1] . Since each group member's software competence is different and the project is mainly based on simulation and analysis in different software, some group members who do not have proper knowledge on software might lag the project or put more work-load other group members who are good at that.

The eighth point says "to treat fairly all persons and to not engage in acts of discrimination based on race, religion, gender, disability, age, national origin, sexual orientation, gender identity, or gender expression" [1] . Rather than discrimination, some misunderstanding might arise in the project since two supervisors with dif-

ferent specialties are involved. The proposals of both should be taken into account considering different viewpoints on the problem.

1.5 Sustainability and Ethic Issue

The usage of wind energy to produce electricity is one of the most sustainable way to supply the energy demand. Thus, any improvement which will increase wind turbine performance and make them to operate more will contribute the sustainability.

The current in the bearings causes much more maintenance and it raises up safety problem. Since the wind turbine structure is huge, high and the nacelle is full of chunky mechanical equipment, to go top of it and work there is dangerous factor for workers. If the maintenance need can be decreased, those workers would not have to work there too often, or, safety clothes and special climbing shoes are equipped for the workers, and forbidden to enter the nacelle while the wind turbine is operating. These methods can avoids the risk of workers' life. So, the problem on working condition can be considered as an ethic issue.

There are also some environmental effects of wind turbines. Since wind farms are spread to wide area, they interrupt migration path of birds. The blades are really long and diameter of a turbine can be up to 100 m, during the operation those blades hit birds flying around and kill them. Some of birds species which are in danger extinction can be affected. Moreover, during summer because wind turbine nacelle is warm, many insects live on it and bats try out to eat them by flying around the turbine. As it can be guessed, blades might kill bats which is not ethic in environmental aspect.

In addition, If a wind farm was built in a place where inhabitants live around, the noise of the operation could disturb those people. Even if wind energy is sustainable, those effects have to be taken into account.

2

Theory

2.1 Wind Turbine Electrical System

2.1.1 Perspective on some of electrical components in the wind turbine.

The intent of this section is to enlighten the reader with general knowledge about electric system arrangement in the wind power plant. The connection of electrical components and main function of each component are outlined in this section.

The main electrical components found in the wind power plant are shown below in Figure 2.1.
a) Generator: This is a electrical machine which converts mechanical energy into electrical energy. Its input is mechanical energy from main shaft and output is electrical energy which is connected to the frequency converter by the cables.

b) Due to mismatch between generator frequency and grid frequency, a frequency converter is used. The frequency converter has a rectifier and inverter circuits. The rectifier, converts the incoming AC from generator to DC, and then the inverter circuit converts DC back to AC with the frequency matching the grid frequency.[2].

c) Transformer: A transformer does the job of stepping up the voltage to match the grid voltage before being fed to the grid for transmission.

d) Electrical cables: Electrical cables enable the flow of power all the way from the generator to the grid. In other words, cables connect all electrical components and allow electrical power to flow.

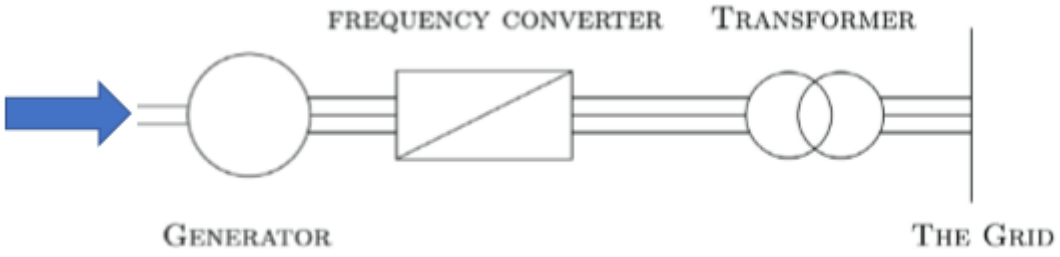

Figure 2.1: Electrical system [2]

In addition to components mentioned above, nacelle is packed with other electrical components for instance pitch control system which is made of several motors that control blades to achieve optimal position and speed.

However, in this part, electrical cables and grounding system will be discussed in a more detailed way simply because

1. In the simulation part, the influence of current carrying cables was investigated and this is what makes cables a point of concern in this work.

2. During measurement it was found that there is current flowing in the grounding cables. Therefore, it is important to discuss grounding system mostly for the benefit of the future work to give an orientation on how to proceed with the investigation.

Sufficient information will be provided to understand the basics of both electrical cables and grounding network in the electrical power system.

2.1.2 Power Cables

Power cables are utilized to transmit electricity in wind turbine nacelle, and the underground electrification using insulated cables will be introduced.

At first air was used as a major insulating material. Due the need of higher voltages in transmission and distribution, insulation system was forced to develop until recently when new materials like XLPE was invented.

The main parts of the power cables consist of a conductor, electrical insulation surrounded by two layers of semiconductor and the jacket. The main parts are depicted in Figure 2.2.

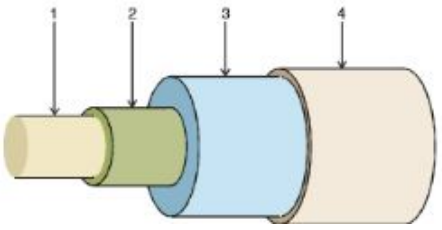

Figure 2.2: Power cable with (1) Conductor; (2) Inner semiconductor layer; (3) Insulator; (4) outer semiconducting layer [3] .

2.1.3 Magnetic field around current carrying conductors

For every current carrying conductor,including power cables there is magnetic field around it. Since magnetic field around any current carrying conductor largely depends on the magnitude of the current, it therefore means that the magnetic field created may influence the surroundings of the cable depending on the magnitude

of the current, and the magnetic field direction around the conductor is shown in Figure 2.3.

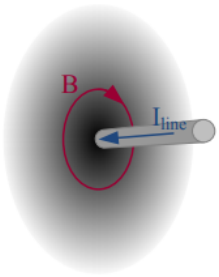

Figure 2.3: Magnetic field around current carrying material [4].

The magnitude and nature of magnetic field around the cables depends on a number factors, such as:

1. Current magnitude, phase balance and/or grounding system.

2. Cable construction parameters such as type and design of the shield

3. External factors like presence of nearby conductors or other current sources.

However a lot has been done in magnetic field management techniques in cables structure [5] , aiming at minimizing the effect of the magnetic field around the cable.

If one of the techniques or all of them are not well designed and applied the magnetic field around cables will obviously be present and most probably it will interfere with surroundings for instance if there are metallic objects around, it may induce some currents or voltage due to electromagnetic induction.

2.1.4 Grounding System

Grounding plays two main roles in electrical system, first it is used as the protection method, in addition to the safety reasons it also sets the reference point in the electrical system. In electrical power system network due to internal, unbalanced faults or by external sources, such as lightning, large fault current may occur into the system. This fault current is very dangerous to both safety of people who work in the area and/or to the electrical components especially the most sensitive ones for instance transformer and generator. Therefore, grounding systems' purpose is to disperse fault currents into the grounding to achieve the safety of workers and components.

The performance and behavior of grounding system depend on many factors, including the physical characteristics of the cables that form the grounding network (material, dimension, and shape etc.), the nature of the soil, grounding method and

magnitude of surge current. [6]–[9].

In addition to the safety of people and components, grounding system also ensures continuous flow of power. A well-functioning grounding system is therefore a big deal in electrical power systems, that is why before installation of the grounding system, it is required to conduct a reliable and efficient study to determine the most important parameters of the system, which are the equivalent resistance of the system and potential distribution on earth surface when the fault current flows into the soil. If these two parameters are not well determined during design, one would compromise the network and the system would be operating on risk of failure any time. Several numerical formulation, theories and models have been put in place to help determining two parameters mentioned above has shown to be highly effective. Therefore, before installation one should first conduct an intensive study to know the type and method that is relevant to avoid possible problems in future [10], [11].

2.2 Magnetic Principles

Magnetism is a phenomena which can be found in many forms. For instance, even the earth has its own magnetic property. The simplest magnetism example can be a permanent magnet found in nature easily. A magnet consists of two poles, north (N) and south (S), and magnetic field lines leaving from the north pole and going into south pole occur around the magnet. Also, as a simple magnetic rule, the same poles propel each other and different poles attracts. The reason of that is magnetic field lines direction and their tendency to align from north to south. Moreover, this is the reason of which a magnet attracts any metal object. Due to the magnetic field, metal object's molecules tend to align as the same as that field and an attraction force takes place between two objects.

2.2.1 Faraday's Law

Faraday's law is the essence of the magnetic phenomena. If a current-carrying conductor is considered, a magnetic field occurs around the conductor. The direction of the magnetic field can be determined by the current direction and the right-hand rule, where thumb aligns current direction and other fingers wrap around the conductor to show the magnetic field direction. With clear understanding of how magnetic field is created, one can figure out Faraday's law in a better way. Faraday's law indicates that if there is a close loop created by a conductor, as long as the time-changing magnetic field exists inside the loop, a voltage can be induced. In mathematical sense, the formula is given below

$$E = -\frac{d\phi}{dt} \tag{2.1}$$

where E and ϕ represent induced voltage and magnetic flux which is proportional to magnetic field and depended on surrounding media.

2.2.2 Rogowski coil

The Rogowski coil is a current transducer that is used for current measurements. The Rogowski coil consists of a wire wound around a non-magnetic core. The core and the windings surrounding it can be wrapped around a conductor where its current is intended to be measured. This transducer transforms the current signal into an output voltage signal. Figure 2.4 depicts the schematic of a Rogowski coil and the external circuit.

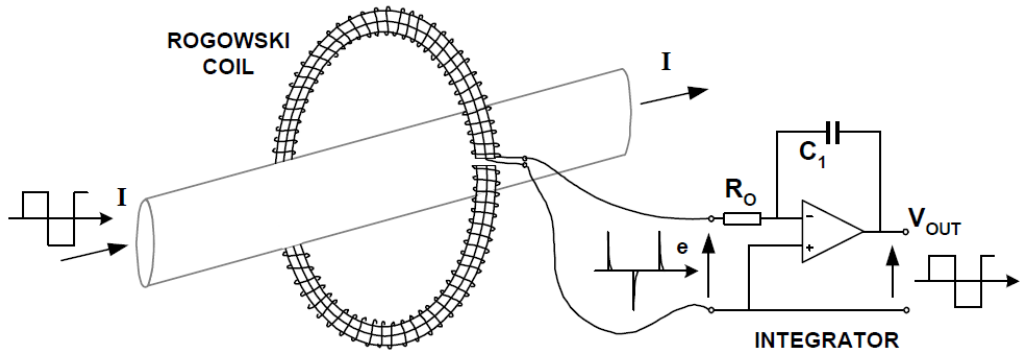

Figure 2.4: Rogowski coil and the integrator circuit for shaping the current [12]

The voltage on the terminal of the coil can be calculated as

$$E = \mu_0 N A \frac{di}{dt} \tag{2.2}$$

where N and A are the numbers of windings and the cross-section of the non-magnetic core respectively and μ_0 is the permeability of free space. However, it can be seen that the output voltage of the coil is proportional to the derivative of the current. Therefore an integrator is required to shape the current [12]. The integrator can be implemented by Op-Amp circuit and RC network as depicted in Figure 2.4. The output of the integrator is proportional to the integration of the input signal and can be presented as

$$V_{out} = \frac{1}{C_1 R_o} \int H \frac{di}{dt} = R_{SH} I \tag{2.3}$$

where C_1 and R_0 are the capacitance and the resistance of the integrator circuit. R_{SH} denotes the sensitivity of the transducer in (mV/A) and is given in the manufacturer specification document. Another important thing about the Rogowski coil is the frequency response of the transducer. Figure 2.5 shows the frequency response of a Rogowski transducer for sinusoidal signals.

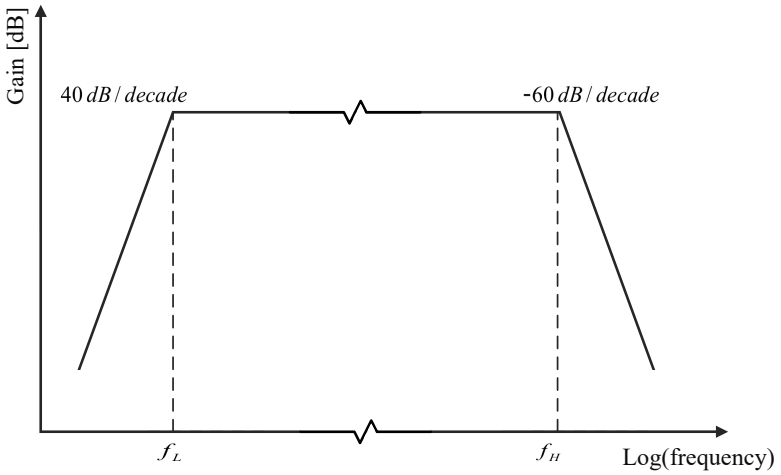

Figure 2.5: Frequency response of the Rogowski coil

f_L and f_H are the low-frequency and high-frequency cutoff frequencies respectively. The gain of the transducer is almost constant and independent of the current location inside the coil as long as the frequency of the measured current lies between f_L and f_H. Below the f_L and above the f_H the gain of the transducer starts to decrease thus affecting the measurement results.

2.3 Mechanical Structure

A wind turbine has an advanced mechanical structure consisting of some components such as blades, nacelle, and foundation in a general aspect. Figure 2.6 illustrates main parts of a wind turbine. Blades are used to catch wind energy due to their special aerodynamic design; the hub connects those blades and it is connected to the shaft which conveys the mechanical energy into the nacelle. The circular area created by blades and the hub has a diameter which is called rotor diameter depending on the desired power capacity of the wind turbine. The larger diameter, the higher energy can be harvested from blowing wind. For example, while a wind turbine with 50 m diameter produces 600 kW, another one with 125 m produces 5000 kW approximately.

The nacelle is the part which includes almost all electrical components of the wind turbine and it is mounted on the top of the tower. There is a component called yaw system between nacelle and tower which allows blades to align to change wind direction. Therefore, more wind energy can be caught even if the wind direction changes.

Foundation is a concrete basement on which the tower is erected. It stabilizes the whole structure in case of any excessive external force.

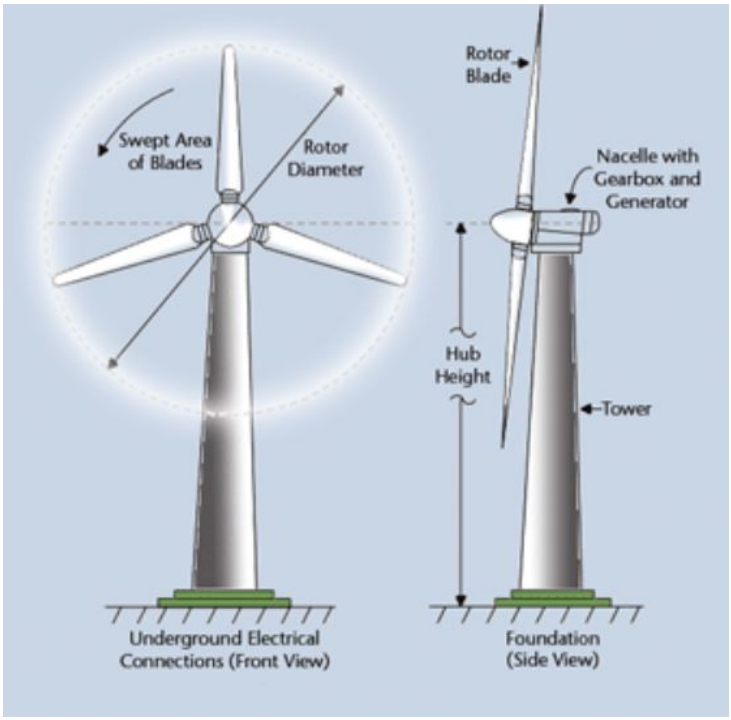

Figure 2.6: Wind turbine overall structure [13]

2.3.1 Nacelle structure

In a wind turbine, the energy conversion from mechanical to electrical takes place in the nacelle. A nacelle basically consists of gear box, generator, converter and sometimes transformer. In Figure 2.7, it is shown how components in the nacelle are located. The gear box alters the relatively low rotational speed to high speed for the generator. The generator produces electricity by using that rotational force. A converter which is named as control electronics in Figure 2.7 adjusts voltage and current waveforms and frequency to be able to connect and transmit that produced electrical power to the grid.

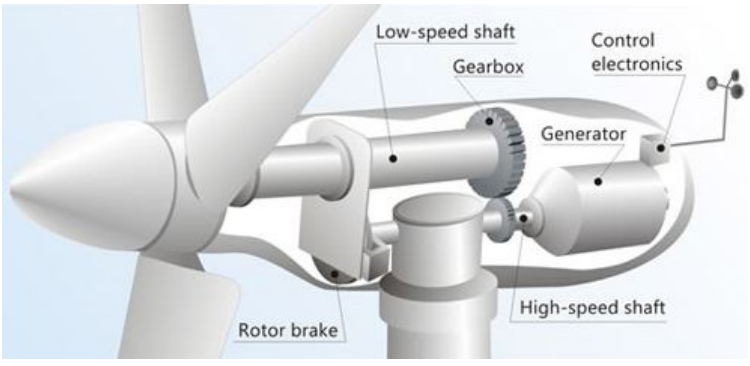

Figure 2.7: Simplified nacelle structure [14]

Big Glenn wind turbine which will be investigated in this projects includes a transformer in its nacelle unit but it does not have any gear box since a permanent

magnet synchronous generator is used. Also, the generator takes large place in the nacelle due to its structure which is designed to handle a very large torque at low speed rotation. In addition, the shaft and bearings are covered by nacelle unit.

2.3.2 The Bearings

Bearings are the components which enable the shaft of wind turbine to rotate in a fixed axis. Thus, it plays an important role in the energy conversion. In any case of damaged or worn off bearings, mechanical efficiency could be decreased in a distinguished way and some electrical issues might arise like undesired current in them. In Figure 2.8, a bearing is shown. Blue part of the bearings is called foot and used to assemble it to the basement of the nacelle. The large cylinder is a shaft connected to any rotational unit, and it can be wind turbine shaft, generator shaft and etc. The shaft is covered by a circular component which includes many small cylinders between outer race and inner race.

Bearings are made of different materials which are either conductive or non-conductive. For example, stainless steel, chrome steel, and ceramic are common materials in bearings manufacturing. In the bearings structure, a lubricant, mostly oil, is used between those small cylinders to decrease friction and make the rotation easier. However, those materials selection might affect electrical system in the nacelle since the lubricant and bearings can behave as a capacitor under a certain amount of voltage. Because of that, some discharges or continuously flowing current which cause damage and worn off could occur on the bearings.

Figure 2.8: Bearings of a wind turbine [15]

3

Methods

Some measurements are performed in Big Glenn site with the aim of identifying possible sources of the currents in the bearings. The proposals for the possible sources of the currents are simulated and studied with COMSOL. The measurement set-up and procedure are presented in subsequent sections followed by the simulation approach.

3.1 Electrical Components and Circuit Diagram of the Nacelle

In this section, single line electric diagram of Big Glenn will be introduced. Figure 3.1 shows the diagram below. At the bottom of the figure, generator outputs are illustrated. There are two groups of output connected to two converters. Between the generator and converters there are some protection devices and also after converters those devices are set up to prevent any damage due to the over-current. In the output of the converters, there are some relays as well. After those breakers a transformer which increases the voltage from 0.69kV to 10.8kV is connected to them. The output of that transformer goes to tower base which includes breaker, at the top of the figure. Furthermore, at the right hand side of Figure 3.1, a transformer fed by the generator is shown. The transformer provides energy to other equipment in nacelle such as induction machines for yaw and the pitch control and cooling system.

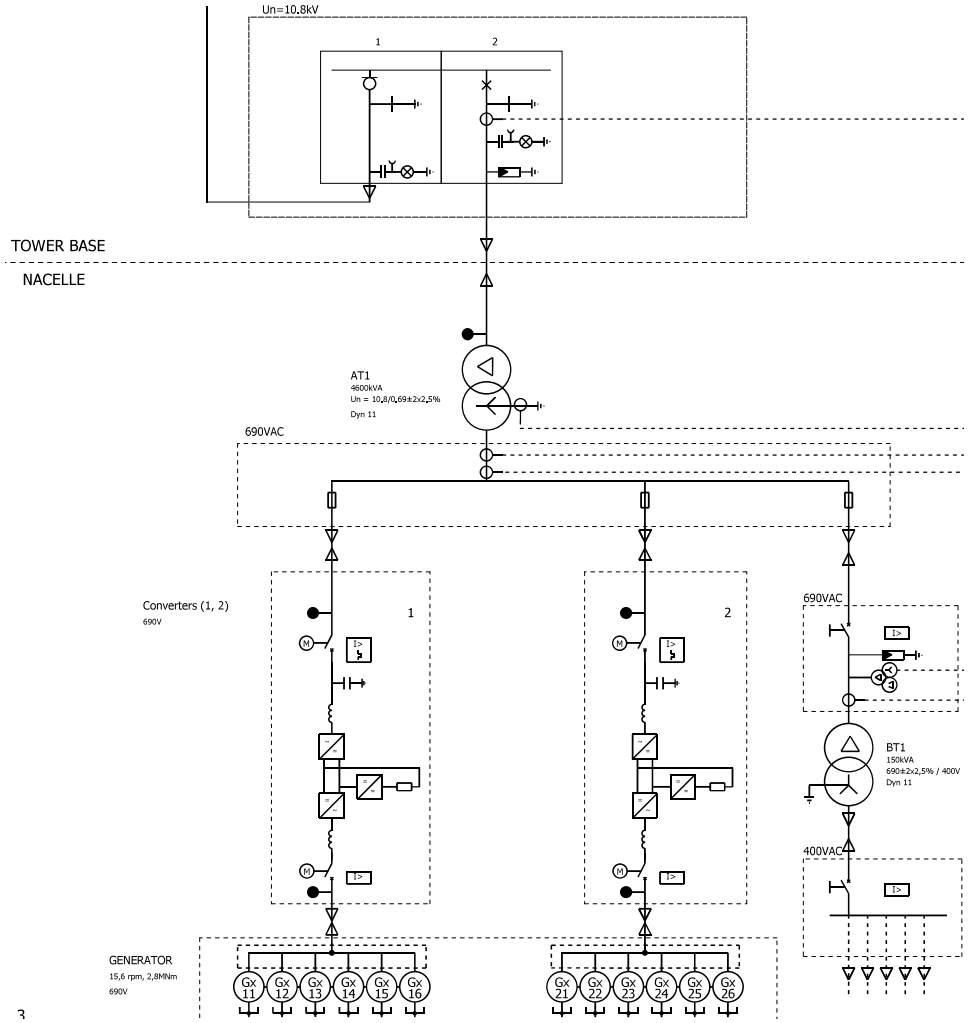

Figure 3.1: Single line electrical diagram [16]

3.2 Electrical Measurement Set-up

Measurements were performed on the site of the Big Glenn wind turbine to identify the possible source of the currents in the bearings of the wind turbine. Figure 3.2 shows a rough sketch of the mechanical and electrical equipment of interest inside the nacelle that the measurements were performed on.

The power is transferred from the generator to the converters with a set of 18 power cables. The output of the converter is 50 Hz AC which in-turn feeds an mega volt transformer. All equipment on the generator housing is grounded, and the ground cables are gathered on a single bus which is denoted here with the generator ground.

The Rogowski transducers were utilized to measure the current flowing through components. The number of the Rogowski coils available and the length of the coils were two limiting factors to opt red-marked points on the Figure 3.2 as measurement points. The measurements points on mechanical components are limited by

the fact that only two Rogowski transducers with length of six meter was available. So it has been decided to measure the current pathing through the bearing near the generator and on the shaft. In this way, the current coming from the generator side and pathing through the shaft can be obtained by applying the Kirchhoff's current law on the node connecting these components. The Rogowski coils are placed in a way that the direction of the current they measure is as depicted in Figure 3.2; thus the sum of the currents on the shaft and the foot of the bearing near generator will provide the current flowing from the generator toward the bearing.

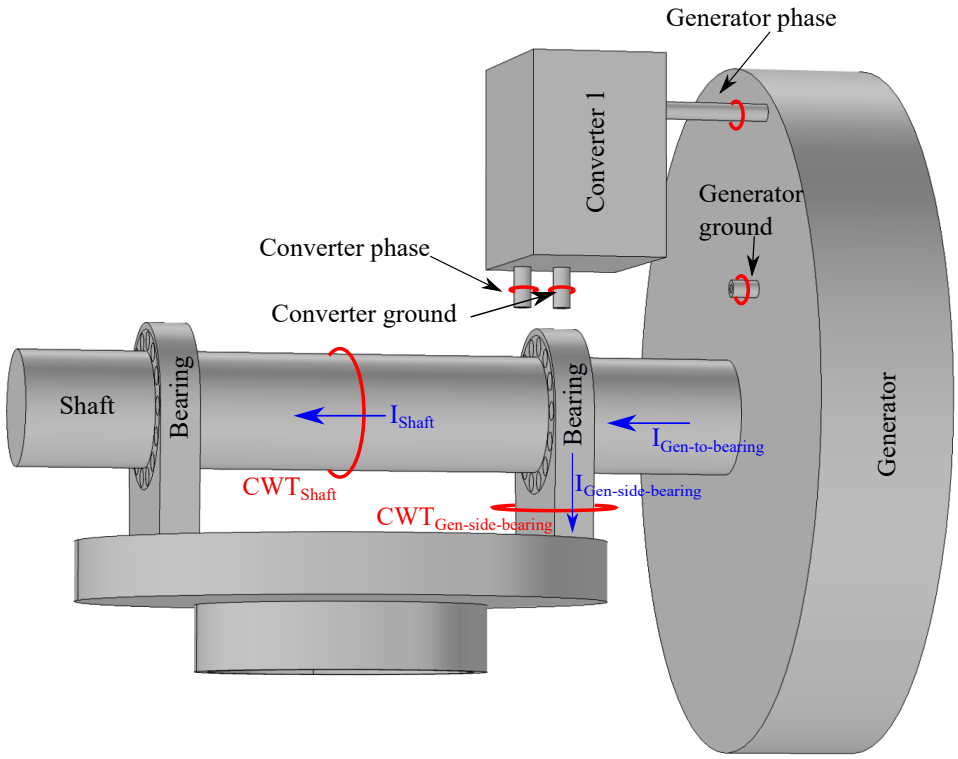

Figure 3.2: Nacelle components and the measurement points at Big Glenn site on November 15^{th} 2017

The grounding system was one of the suspected culprits. Therefore two of the Rogowski coils are dedicated to measure the currents in the grounding cables of the generator and converter as shown in Figure 3.2. To have reference signals the generator and the converter phase currents were also measured using two sets of Rogowski coils.

Rogowski Current Waveform Transducers (CWT) from PEM company was utilized to set up the measurement system. The CWT3 which is a standard type Rogowski coil with the sensitivity of 10 mV/A was utilized. According to manufacturer datasheet, the low-frequency cut-off frequency of the transducer is 3.5Hz; Therefore, in order to transform the measured voltages from the transducer to respective current waveforms the nominal sensitivity can be used down to 3.5 Hz. Depending on the length of the coil the high-corner-frequency of the transducer varies between

10-16 MHz which are irrelevant frequency range for the grid-frequency or the high-power power electronic applications.

Figure 3.3 shows the placement of the Rogowski coils around the phase and ground cables of the generator and the converter in the Big Glenn nacelle. The outputs of the CWTs are connected to High-precision PC oscilloscope PicoScope 4824 through BNC cables to record the measured data. PicoScope 4824 can receive eight input signals at the same time through 8 input channels A to H. Six channels are already filled with current signals from CWTs.

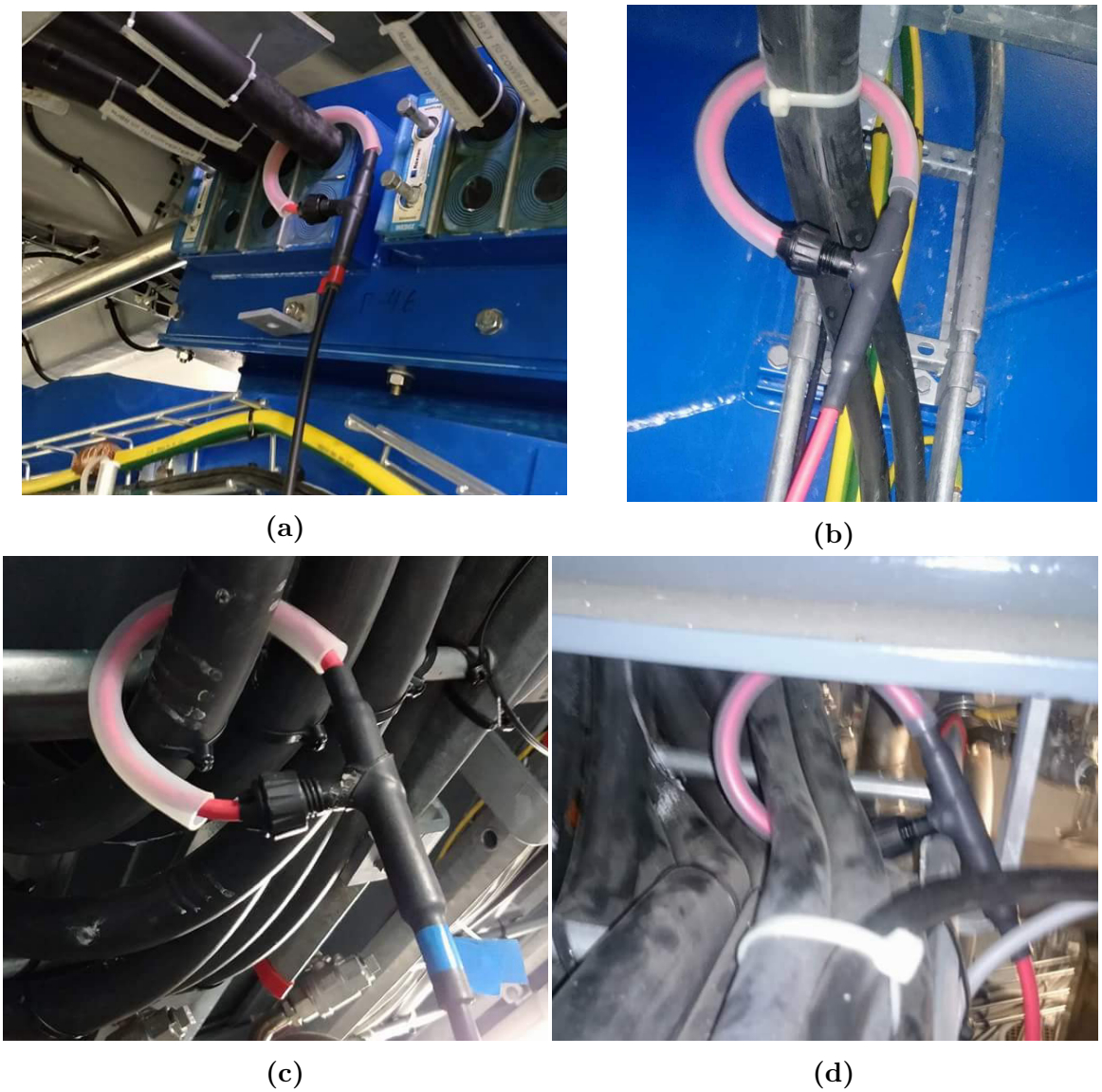

(a) **(b)**

(c) **(d)**

Figure 3.3: The CWT placements on the Big Glenn Nacelle (a) the generator phase current (b) the generator ground current (c) the converter phase current (d) the converter ground current

Another hypothesis was that the magnetic leakage flux from adjacent cables in the

air is the source of the currents in the bearings. Therefore, a loop made of wire is placed above the shaft to catch the flux near the shaft. Another one is placed between the generator and the transformer to investigate the presence of flux around the shaft. Figure 3.4 shows the voltage loops near the generator and above the shaft.Two ends of the yellow wires are connected to Picoscope through BNC cables.

The measurements are performed at intervals of 10 seconds with a number of one million samples. Therefore, the sampling frequency is 100 kHz and frequencies up to 50 kHz can be detected successfully by applying Fourier transformation on the waveforms.

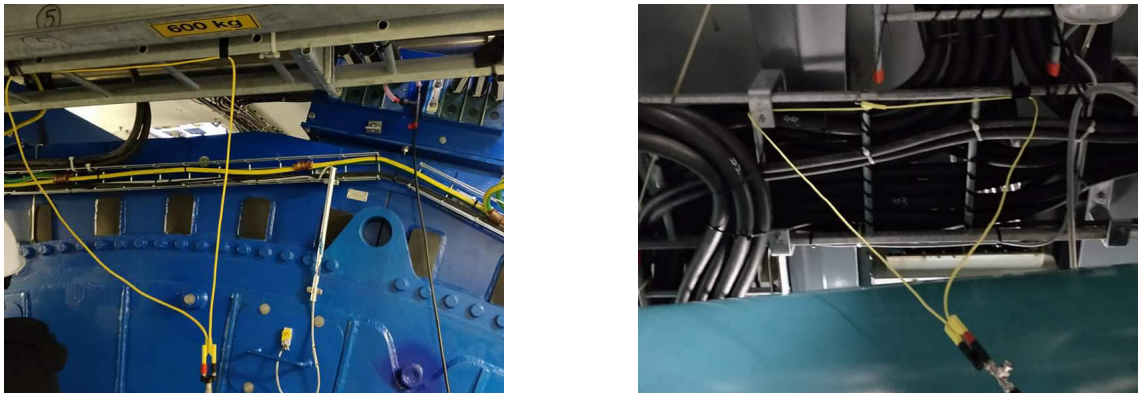

(a) **(b)**

Figure 3.4: The voltage measurement loops at Big Glenn site (a) near the generator (b) above the shaft

The data obtained from Picoscope was imported into Matlab. The FFT function of Matlab was used to obtain the single-sided amplitude spectrum of the signals. The Matlab codes to perform the Fourier transformation on the signals can be found in Appendix A.The measured waveforms along with amplitude spectrum are presented in section 4.1.

Another set of measurements were performed on the site of Big Glenn on April 11^{th}, 2017. The group was provided with the measurements data which were needed to be analyzed in the same manner as previous ones. Figure 3.5 shows the location of current sensors in the nacelle. The currents are measured on the shaft near the hub, on the hub-side bearing, and between the generator and the generator-side bearing as depicted in Figure 3.5. The shaft current and the Generator-side bearing current can be obtained by applying Kirchhoff's current law on the bearings as nodes. The results of the analysis are depicted in section 4.1.

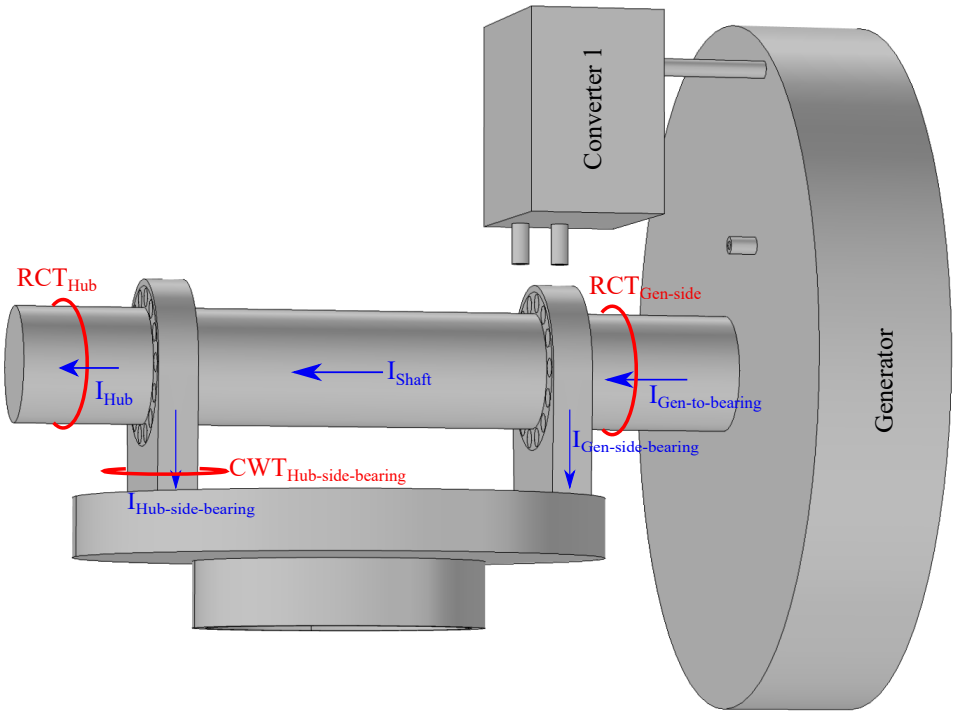

Figure 3.5: Nacelle components and the measurement points at Big Glenn site on April 11^{th} 2017

3.3 Simulation

In this section, the model of electrical parts of the turbine is simulated in COMSOL. With the respect to possible root causes, there are some power cables hanging above the shaft, therefore the induced magnetic field around the shaft is suspicious. The main purpose of doing the simulation is to verify whether this proposal is reasonable or not.

3.3.1 The geometry design

The geometrical measurement data from Big Glenn is shown in Table 3.1.

Table 3.1: Parameter of the nacelle

Parameter	Value[m]	Parameter	Value[m]
Radius of cable jacket	0.065	Width of bearing	0.3
Bearing radius	0.6	Bearing housing radius	0.65
Height of bearing	2.8	Length of shaft	3
Shaft perimeter	2.75	Diameter of nacelle basement	3.6

Some parts of the nacelle were not be able to measure, for example the radius of the steel ball inside of the bearing, the number of steel ball, the distance between

the steel ball and the bearing wall and etc, thus reasonable values of them were assumed. Besides, some mechanical structures such as the steel brackets, the stage for supporting the bearings and the metal collector for power cable above the shaft were ignored. Also, the power cables are simplified to only three phases and the structure of the cable is simulated only with conductor and insulation layer where semi-conductor and outer jacket are ignored. The cables are placed in line with each other to restore the real circumstance in the nacelle. The general structure of the simplified model geometry is shown in Figure 3.6.

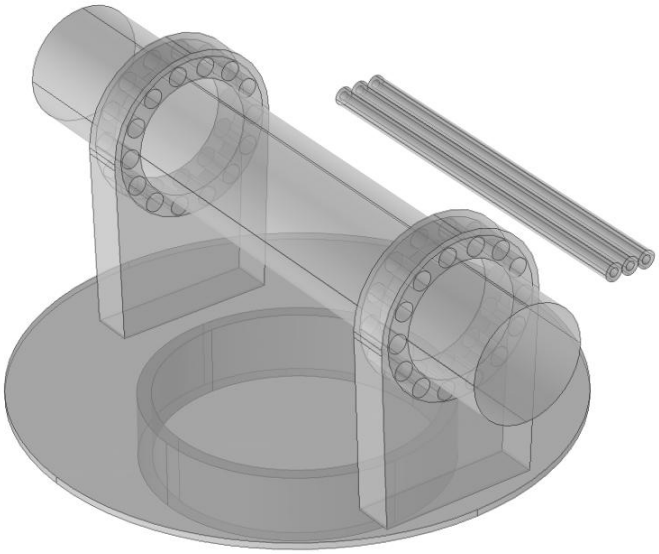

Figure 3.6: Nacelle geometry in COMSOL

In Figure 3.6, generator, transformer and converter are ignored. The three phase cables are suspended in the air right above the shaft, and those cables are coming from the converters. By changing the input current inside of the cable, three phase current with different frequencies, magnitudes and sequences can be modeled. With the respect of bearing, 14 steel balls are embedded into the bearing. The bearing balls and the inner race and outer race are not touched therefore there is a small space for lubricant.

3.3.2 The Materials Selection

The components in the simulation can be divided as cables, bearing, shaft and base. The materials for each of the components are listed in Table 3.2

Table 3.2: Material of the components

Material	Components
Air	Air block outside of the model
Silicon	Lubricants inside of bearing
Structural steel	Bearing, bearing base, shaft and nacelle base
Copper	Conductor of the cable
PVC	Insulation of the cable

In the materials selection, in order to have a electric current loop, the bearing, base and the shaft are simply considered to be made by steel. Since the semi-conductor layer and outer jacket of the cable are ignored in geometry part, only the insulation layer and conductor are considered which mainly affect the magnetic field in the space.

3.3.3 Simulation

In this section, two simulations are conducted. The first simulation is to investigate the magnetic field near the shaft based on fundamental and third harmonics current. The second one is to predict how much voltage on the shaft can generate corresponding measurement current on the foot of the bearing.

3.3.3.1 Magnetic field study

In order to investigate the magnetic field in the air, Magnetic Fields study is selected. For each of the phase, 120 degree phase shifts are added with the respect of time dependent. The three phase fundamental current can be written as

$$i_a = Acos(wt) \tag{3.1a}$$

$$i_b = Acos(wt + \frac{2\pi}{3}) \tag{3.1b}$$

$$i_c = Acos(wt - \frac{2\pi}{3}) \tag{3.1c}$$

where ω is the system angular speed and A is the magnitude of current.

Besides, the third harmonics should also be investigated. By changing the magnitude of the current and adjusting the phase to the same phase position, the third harmonics can be simulated.
With the respect of boundary condition, surface currents are assigned for each of the copper conductor. Finer is chosen for the mesh and 493493 mesh elements are obtained. The mesh geometry of the nacelle is shown in Figure 3.7.

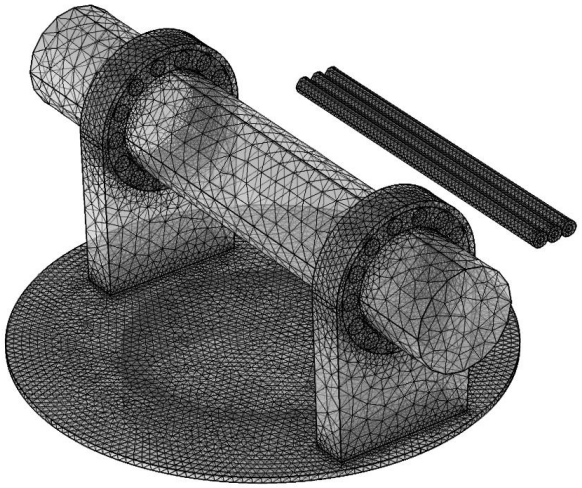

Figure 3.7: Fig:mesh-figure

In order to investigate the influence of the distance between the shaft and the cables on magnetic flux density, parameter sweep is implemented. The geometry of the cable sweep is shown in Figure 3.8

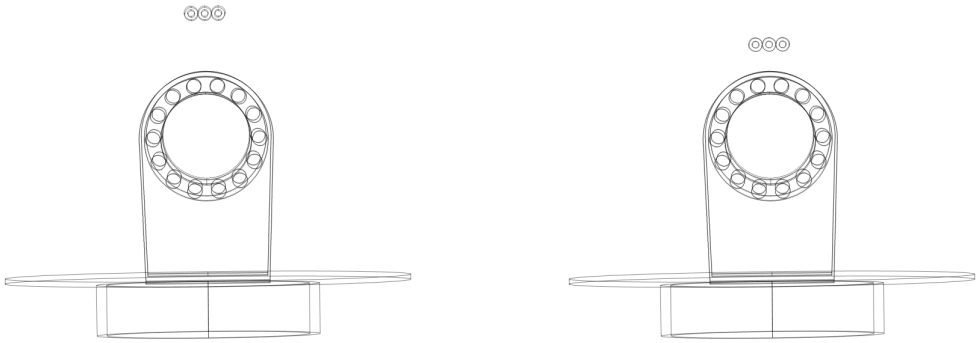

(a) Start point of the cables **(b)** End point of the cables

Figure 3.8: Cable position sweep

The distance variation between each case is 0.3 meters, the main purpose of sweeping parameter is to determine the scale change of the magnetic flux density.

3.3.3.2 Induced voltage determination

The main reason for this part is to investigate and to determine the magnitude of the voltage that can generate the current equivalent to the one we obtained during measurement. The base of bearing is grounded, where as shaft is at high potential as shown in Figure 3.9. The parametric sweep study was computed to determine the voltage that can generate the current equivalent to the measured one.

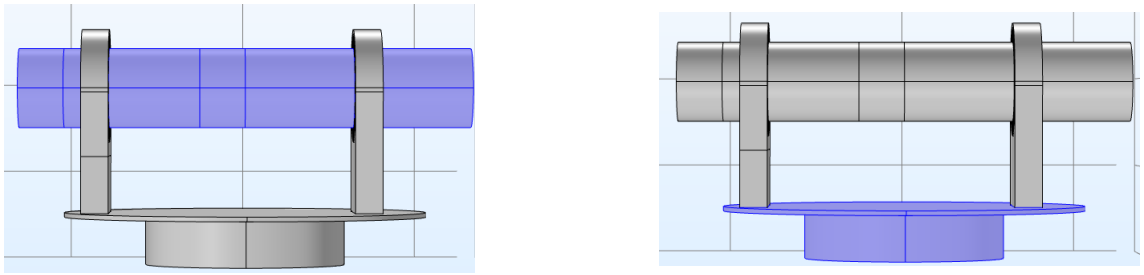

(a) **(b)**

Figure 3.9: Boundary condition (a) High potential, (b) Ground

4

Results and Analysis

4.1 Measurements Results

The data from measurements performed in the Big Glenn site are imported into Matlab. With the help of Fast-Fourier-Transformation (FFT) function of Matlab, the single-sided amplitude spectrum of the signals are extracted and plotted.
Figure 4.1 shows the generator and the converter phase current waveforms and respective single-sided amplitude spectrum for the first measurement performed on November 15^{th} 2017.

It can be seen that main component in the generator phase current is 10.9 Hz frequency which is the frequency of the turbine and the generated voltage. The second, the third, the fifth harmonics are another notable components in the spectrum.

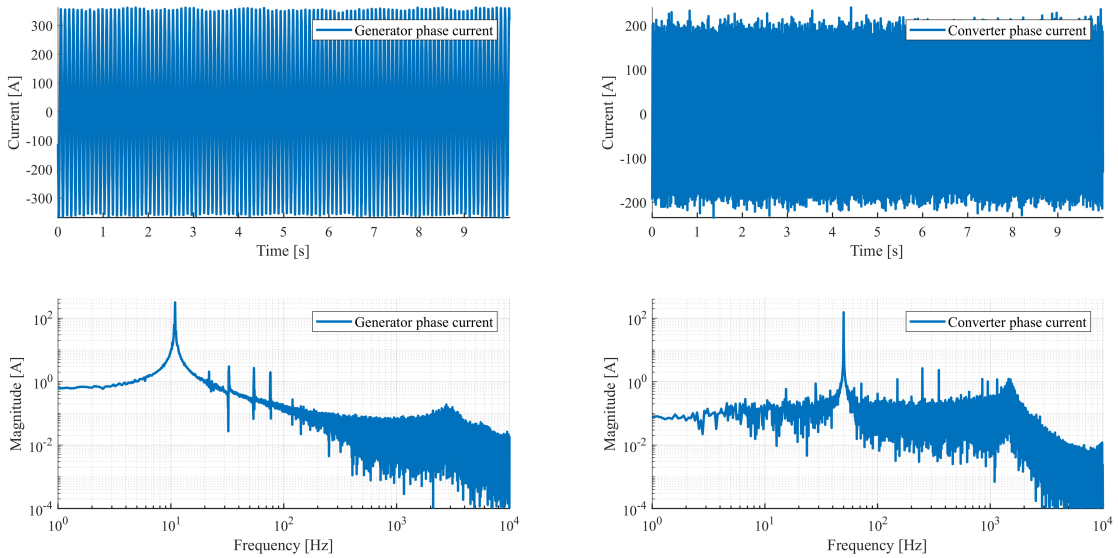

Figure 4.1: The generator and the converter phase current waveforms and the single-sided amplitude spectrum for the first measurement performed on November 15^{th} 2017

On the other hand, the converter is used to change the frequency of the voltage to the grid-frequency; therefore, the 50 Hz is the prominent component in the frequency spectrum of the converter phase current. The third, the fifth and the seventh harmonics can also be noticed readily.

The zoomed version of the generator and the converter phase currents are depicted in Figure 4.2. As can be seen, the dominant component of the generator phase current is 10.9 Hz. While for the converter phase current, the grid frequency is the predominant component.

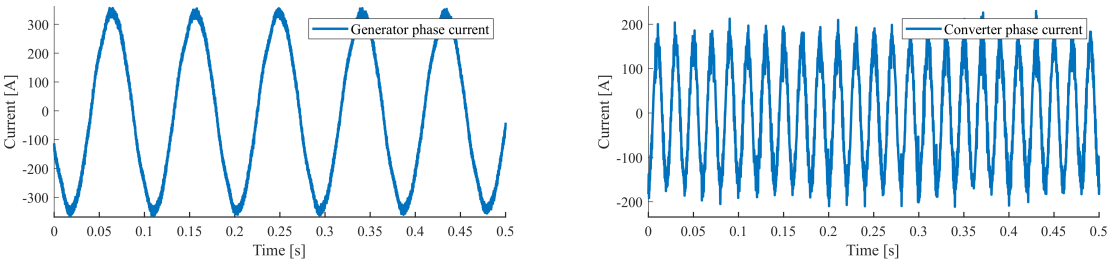

Figure 4.2: The generator and the converter phase current zoomed waveforms for the first measurement performed on November 15^{th} 2017

Figure 4.3 illustrates the current harmonics decomposition in the output cable from the generator for the six consecutive performed measurements. The measurements are denoted with different colors in the graph. The grid frequency (50 Hz) and the generator frequency (the same as the turbine frequency and approximately 10.9 Hz) components are denoted with f_{grid} and f_{Tur} respectively. Superscripts stand for the harmonic order of the respective fundamental frequency. Detailed numbers for each measurement can be found in tables A.1 to A.6 in the appendix.

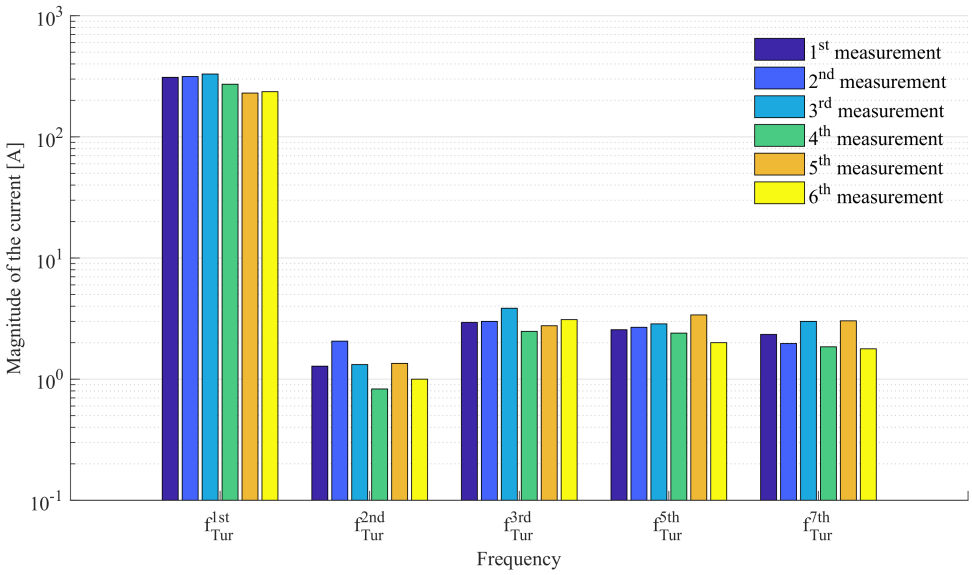

Figure 4.3: the generator output current harmonic contents for different measurements performed on November 15^{th} 2017

Due to the changes in the wind speed between different measurements, the fundamental frequency of the current varies between 10.85 Hz to 11 Hz. For the same reason, the output power and therefore the magnitude of the current varies from measurements 1 to 6. However, in all of the measurements the second, the third,

the fifth and the seventh harmonics also flow inside the cable. Where the second harmonic has the lowest magnitude, and for the rest of the components, the magnitude decreases as the harmonic order increases (except for the third and the fifth measurements).

Similarly Figure 4.4 shows the converter output current harmonics. Apart from the fundamental component, the fifth and the seventh harmonics of the grid frequency are the dominant components in the frequency spectrum in all measurements. The third harmonic also exists with relatively low amplitude compared to the rest of the components.

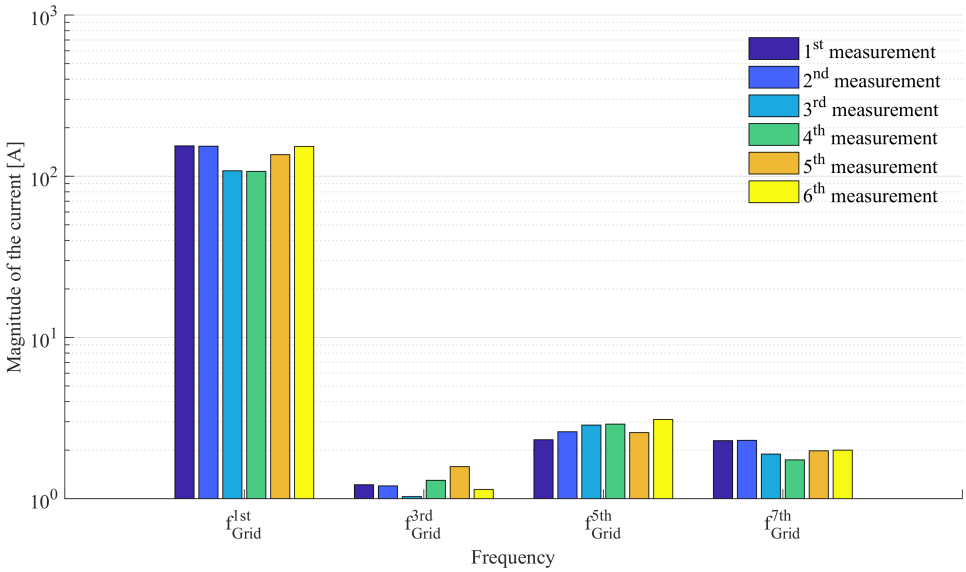

Figure 4.4: the converter output current harmonic contents for different measurements performed on November 15^{th} 2017

As mentioned earlier two Rogowski coils are placed on the grounding cables of the converter and the generator. Figure 4.5 shows the waveforms obtained from these sensors and their respective amplitude spectrum. Even though the peak of the generator ground current rises to 100 Amperes in the waveform, the amplitude spectrum shows that it consists of various harmonics with low amplitude. In contrast, a massive amount of grid-frequency current is flowing inside the grounding cable of the converter as shown in Figure 4.5. Its magnitude reaches up to 74 Amperes.

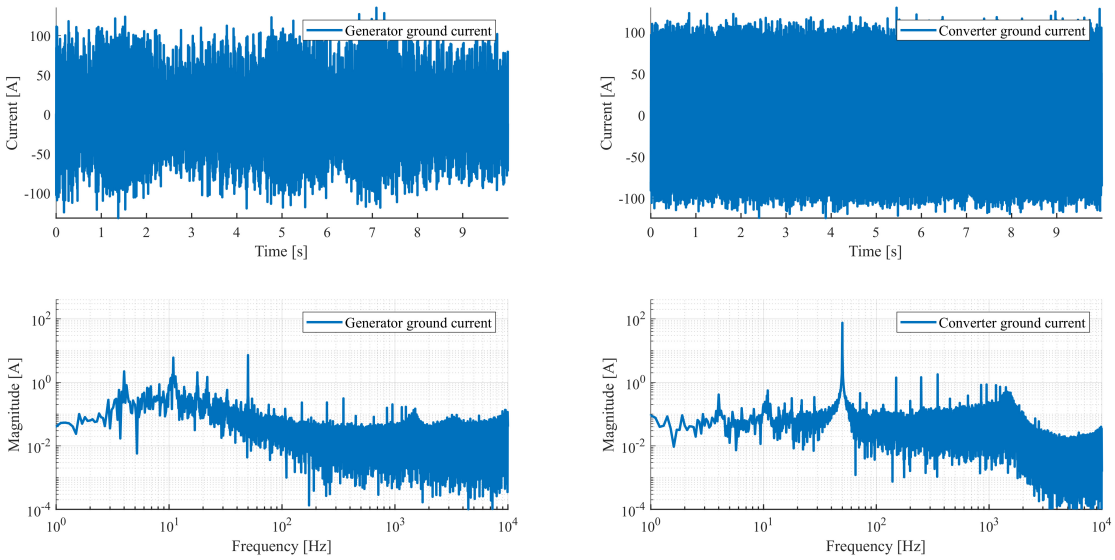

Figure 4.5: The generator and the converter ground current waveforms and the single-sided amplitude spectrum for the first measurement performed on November 15^{th} 2017

The zoomed version of the converter ground cable current is depicted in Figure 4.6; as it is evident the main component of the current is the grid frequency.

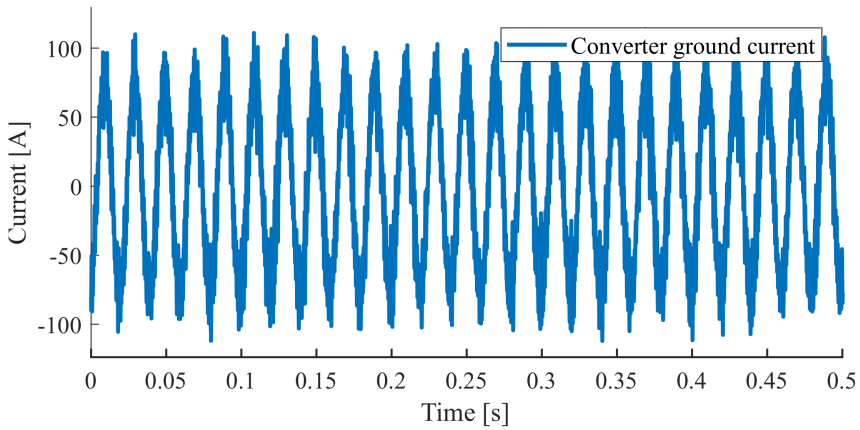

Figure 4.6: The converter ground current zoomed waveform for the first measurement performed on November 15^{th} 2017

Figure 4.7a illustrates the current harmonic decomposition for the generator ground cable. Aside from the grid-frequency and the turbine frequency and their respective harmonics, 4 Hz, 17 Hz, 85 Hz and 106 Hz frequency components can also be found in the grounding cable of the generator. The predominant frequency components are the fundamentals, followed by the 4 Hz and the 17 Hz. The magnitudes of the components are below 10 Amperes for all measurements.

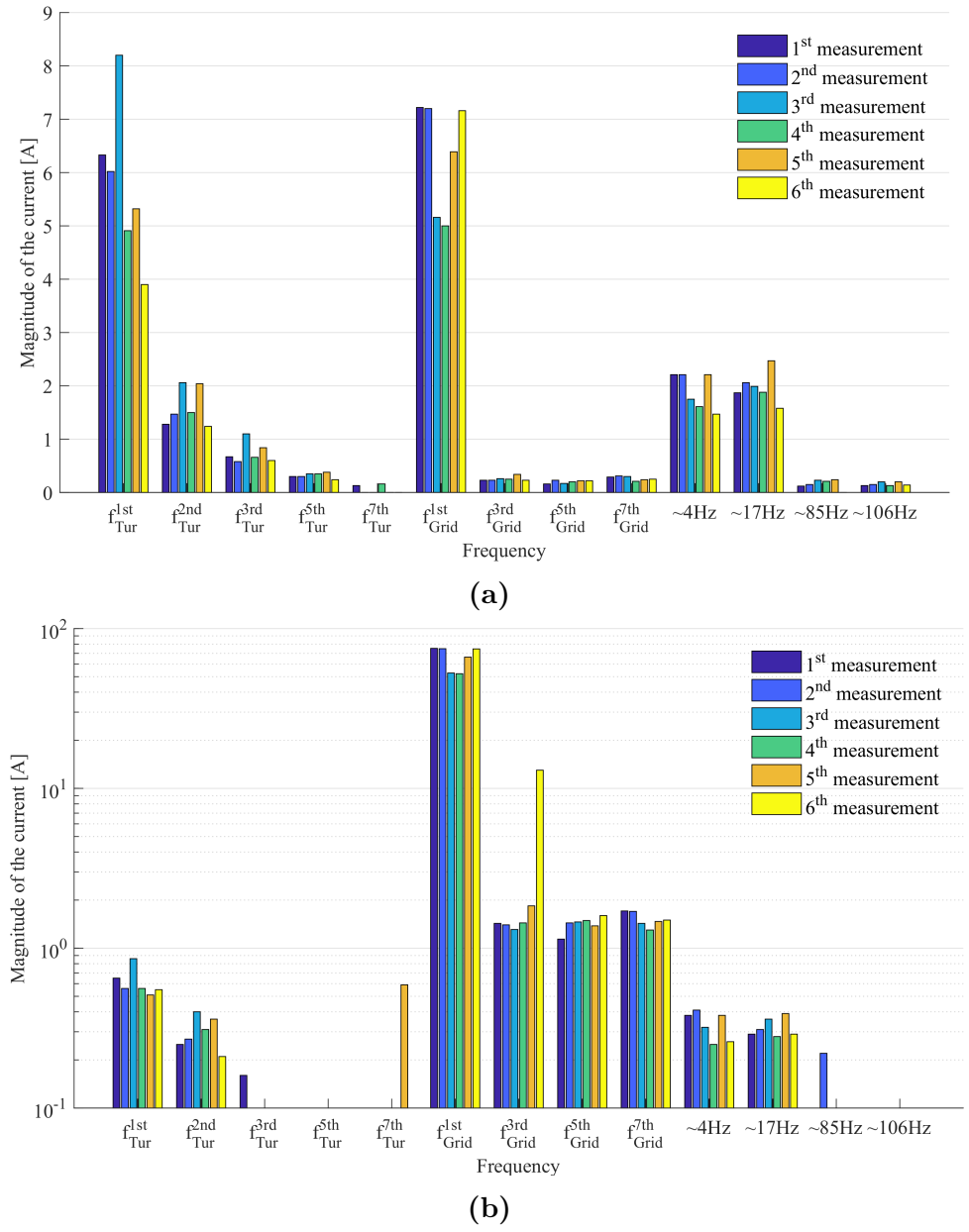

Figure 4.7: Current harmonic contents for different measurements performed on November 15^{th} 2017 (a) generator ground cable (b) converter ground cable

Same as the first measurements, a huge grid-frequency current exists inside the grounding cable of the converter in all of the measurements. Figure 4.7b shows the harmonic contents of the converter ground cable. Apart from the fundamental grid-frequency. The third, the fifth and the seventh harmonics of the grid-frequency are dominating components and are almost in the same range of magnitude.

The induced voltages above the shaft and near the generator are depicted in Figure 4.8. The amplitude of these voltages is below 3 volts. Inspection of the amplitude spectrum does not reveal that much information due to the high level of the noise in the signals. However, for the induced voltage above the shaft, the 50Hz is the dominant frequency component with the magnitude of 0.026 volts.

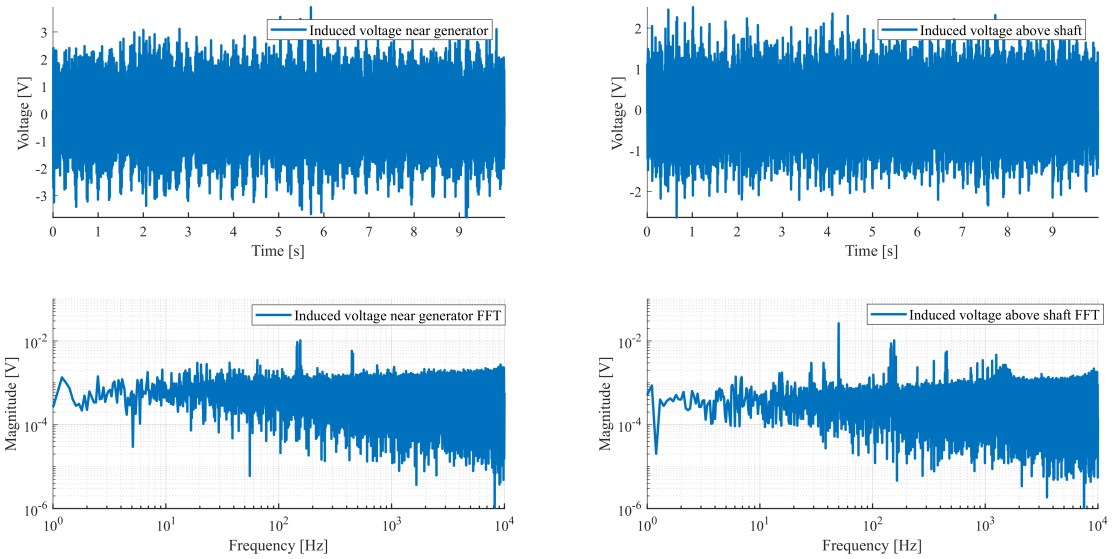

Figure 4.8: The waveforms and the single-sided amplitude spectrums of the induced voltages above the shaft and near the generator for the first measurement performed on November 15^{th} 2017

The waveforms of the currents flowing inside the shaft and through the bearing and corresponding amplitude spectrum and harmonic content decomposition are illustrated in Figure 4.9 and Figure 4.10.

Figure 4.10a shows the currents on the shaft of the turbine between two bearings. The grid-frequency is the main current component of the shaft. Comparison of different measurements in Figure 4.7b and 4.10a shows that there is a direct relation between the magnitude of the current in the converter ground cables and the current on the shaft; Where the current on the shaft is 13.7 ± 0.2 times lower than the current in the converter's ground cable. Also, the magnitude variation of f_{Tur}^{1st} between different measurements has the same trends in the converter ground cable and the shaft current.

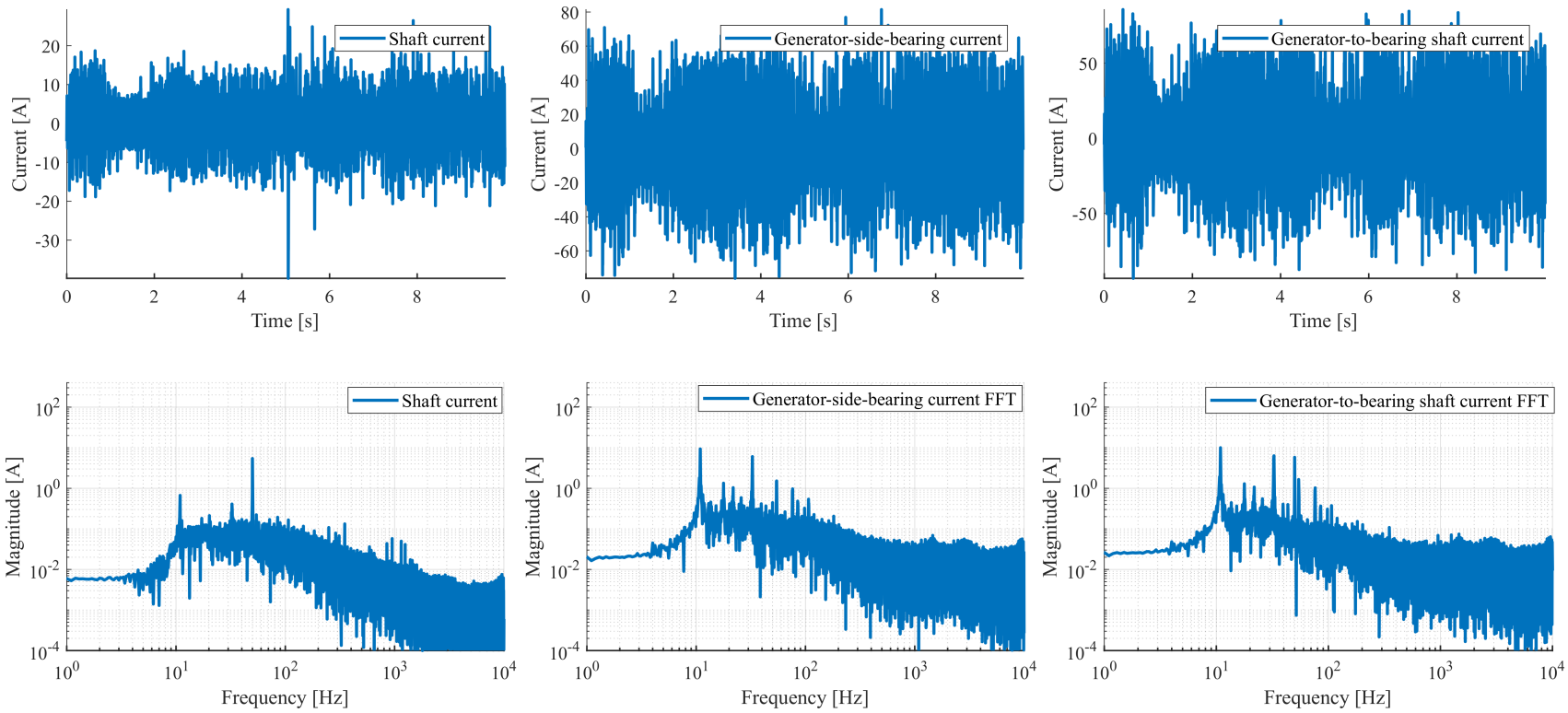

Figure 4.9: The waveforms and the single-sided amplitude spectrums of the currents in the shaft and the current throw the bearing near the generator for the first measurement performed on November 15^{th} 2017

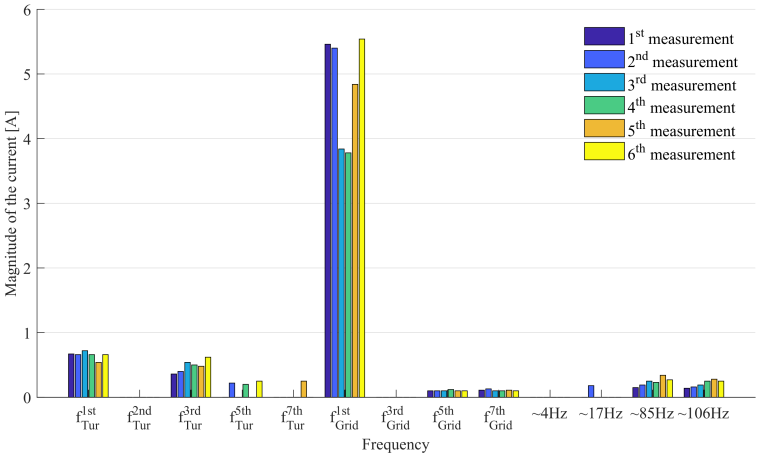

(a) Shaft current

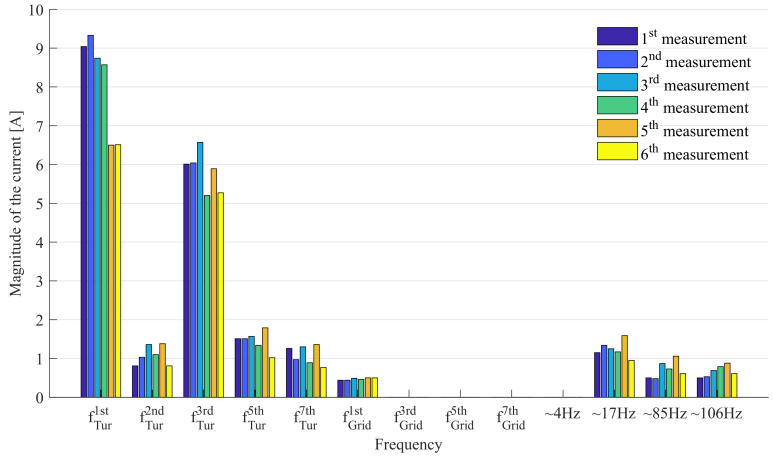

(b) Generator-side bearing current

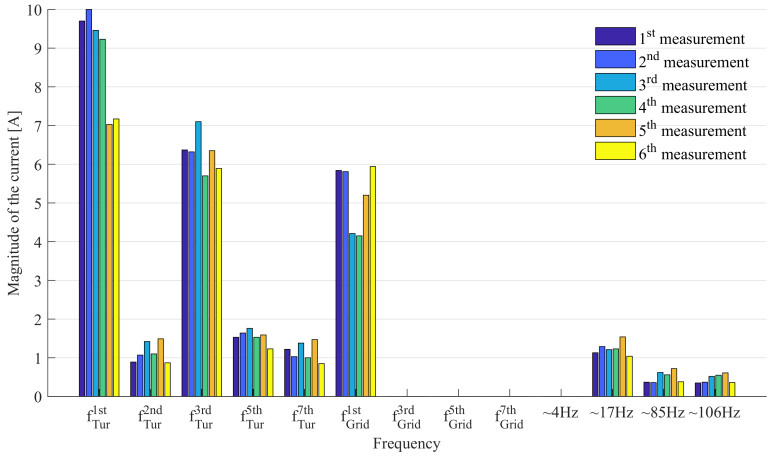

(c) Current flowing from generator toward generator-side bearing

Figure 4.10: Current harmonic contents for different measurements performed on November 15^{th} 2017

Another important point to notice is that both in the spectrum of the shaft current and the induced voltage above the shaft the dominant component is the 50 Hz frequency. Presence of the 50 Hz magnetic field above the shaft could be either due to the currents flowing inside the power cables or because of the current inside the shaft itself. The former itself could be a reason for the currents in the bearings which would be investigated in the upcoming sections in COMSOL software.

Figure 4.10b shows the harmonic content of the current flowing from bearing located near the generator to the tower structure. The dominant components are the fundamental and the third harmonics of the generator frequency. Applying the Kirchhoff's current law on the bearing as a node, the current flow on the shaft from generator side toward the bearing can be obtained as Figure 4.10c.

Harmonic contents of the generator cable for the measurements performed on April 11^{th} are depicted in Figure 4.11. (All the waveforms can be found in Appendix) The first and the second measurements pertain to the start-up phase of the turbine; Whereas the third and fourth measurements relate to the operation of the wind turbine with the speed of 10.7 Hz. The detailed numbers for each of the measurements could be found in Appendix A. The generator cable contains the same harmonics as the measurements performed on November 15^{th}. The magnitudes of the harmonics relative to the fundamental are following the same pattern in both of the measurement sets. However, the magnitude of the second harmonic is slightly higher in the measurements performed on April 11^{th}.

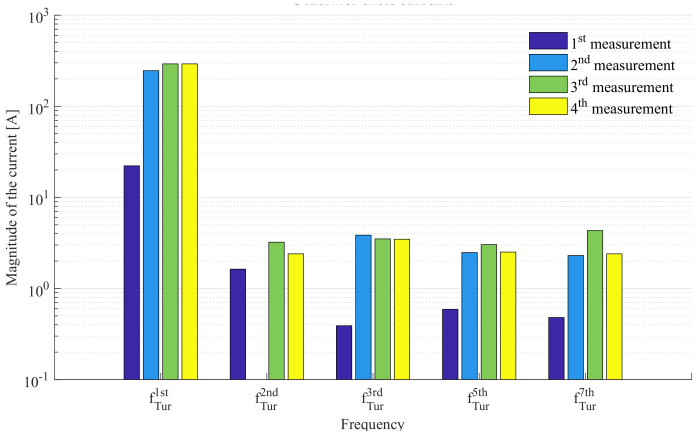

Figure 4.11: Generator current harmonic contents for different measurements performed on April 11^{th} 2017

Figure 4.12 depicts the harmonic contents of the currents on different parts of the turbine shaft and both of the bearings. Also, there is a small correspondence between the measurements performed on two different dates. The dominant harmonics in the generator-side bearing is the same in two measurement sets. However, the magnitudes of the currents are much higher in the measurements performed on April 11^{th}. Besides the magnitude of the third harmonic is higher than the fundamental; which is not the case in the other measurement.

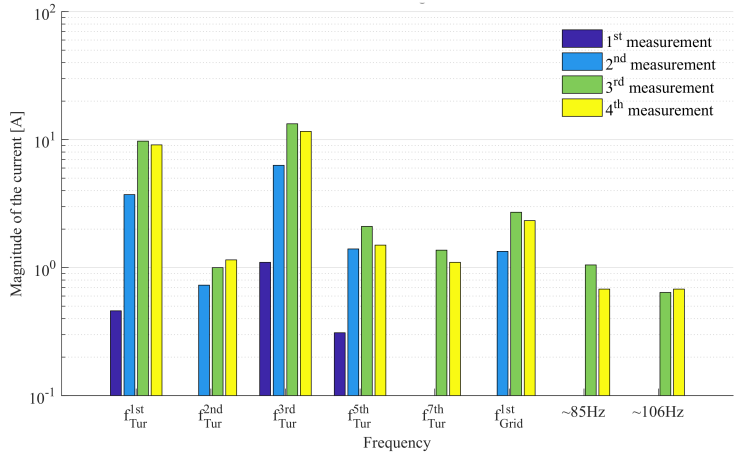

(a) The hub-side bearing current

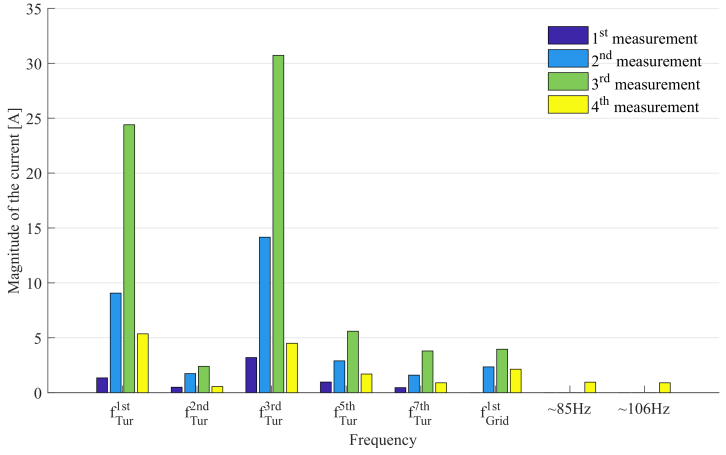

(b) Generator-side bearing current

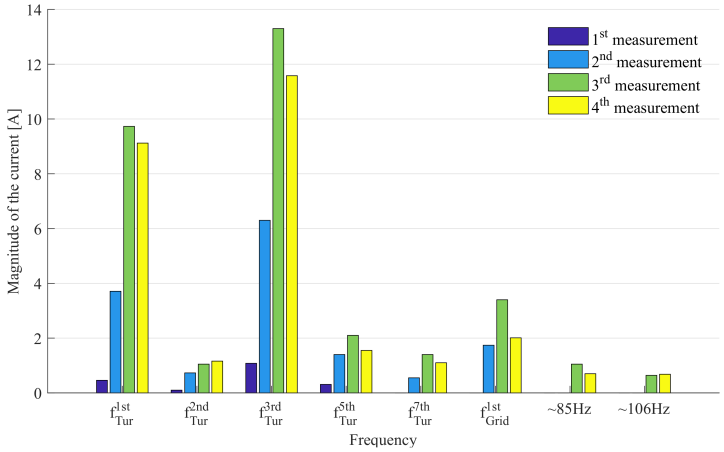

(c) Shaft current

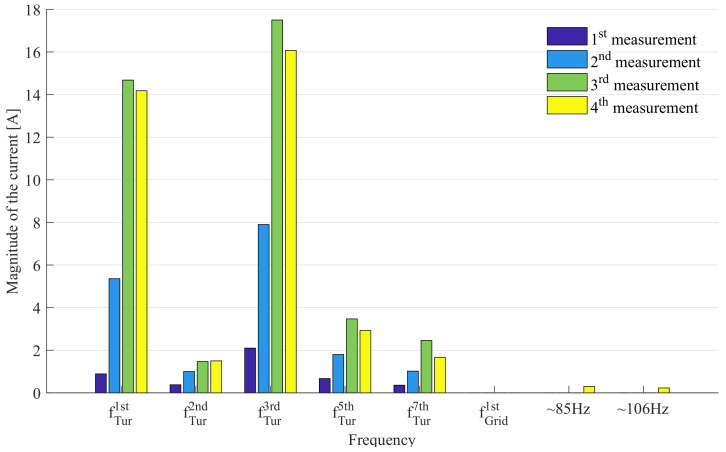

(d) Current flowing from generator toward generator-side bearing

Figure 4.12: Current harmonic contents for measurements performed on April 11^{th} 2017 (Figure(a) is in logarithmic scale)

Figure 4.12c illustrates that the main component of the shaft current is the third harmonic of the generator frequency followed by the fundamental component. In contrast, the main current following inside the shaft was detected to be 50 Hz in the measurements performed on November 15^{th}. As depicted in Figure 4.12d, no 50 Hz current is flowing from generator toward the bearings; which implies that the 50 Hz current is circulating between bearings on contrast to measurements performed on November 15^{th}.

Another anomaly can be detected with careful inspection of different measurements performed on April 11^{th}. In the third measurement, the current on the shaft and the current coming from the generator side flow inside the generator-side bearing, so they add up together. However, in the fourth measurement, the direction of the currents inside the shaft reverse, so the amount of current flowing into the generator-side bearing reduces considerably.

4.2 Simulation Results

4.2.1 Magnetic field study

After computation, the magnetic field around the shaft can be obtained by adding multislice. According to Faraday's law, the current in the shaft can be generated by magnetic field around it. Therefore, the multislice is set on the same height level with the middle point of the shaft. In this case, first, the fundamental current is investigated. The magnetic flux density is shown in Figure 4.13.

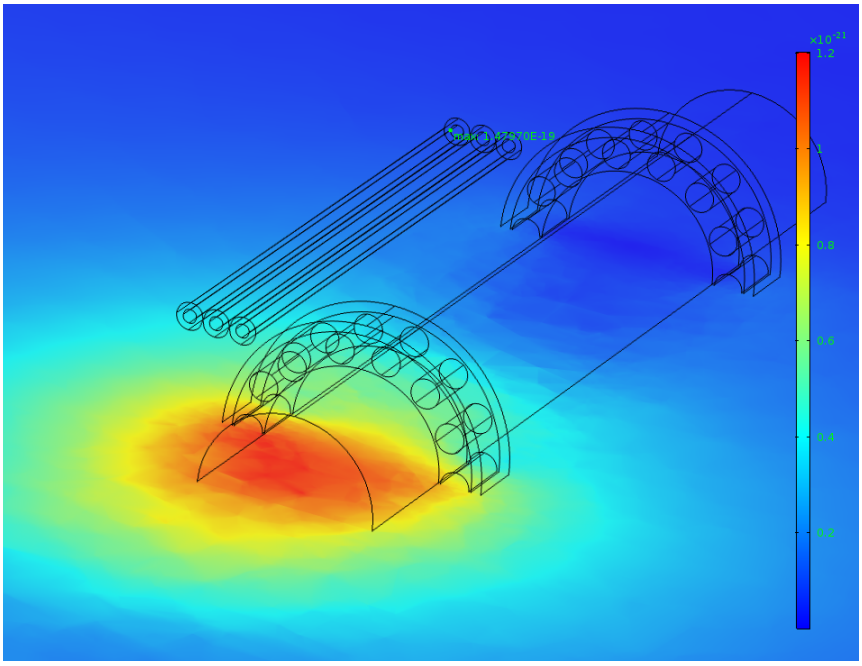

Figure 4.13: Magnetic field distribution near the shaft

In the Figure 4.13, as it can be observed, the magnetic field is concentrated near the

shaft under the power cables. However, the scale of the magnitude is extremely low. The maximum magnetic flux density in this simulation is barely able to be detected. This is mainly because the three phase fundamental currents are cancelled by each other. Thus, in this case, it is not possible to generate any measurable current on the shaft.

Then, the third harmonics are implemented. According to the measurement, the third harmonics of the current coming out of the converter to the generator is near 0.5 Ampere. Therefore, the three phase currents are set as the same as the previous case but with the maximum current of 0.5 Ampere. To simulate the zero-sequence components, the phase shift of 120 degree has been cancelled. The magnetic flux density around the shaft is shown in Figure 4.14

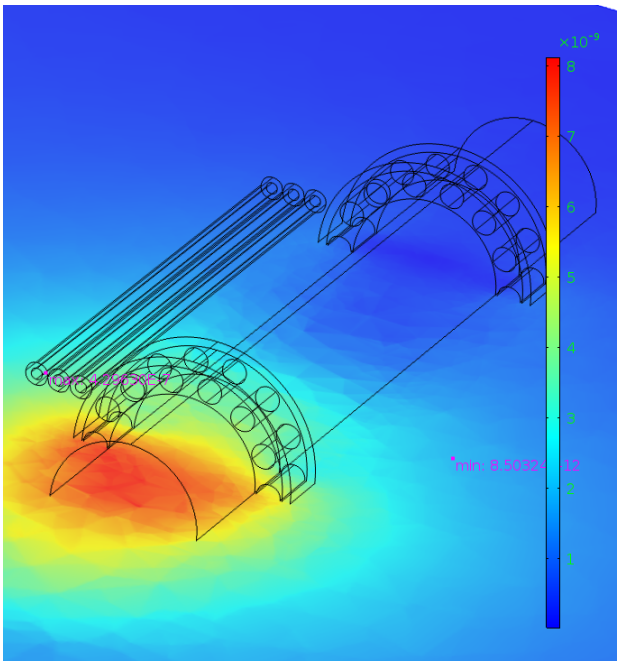

Figure 4.14: Magnetic field distribution near the shaft (3rd harmonics)

In Figure 4.14, the magnetic flux density increased up to the scale of ten to power of minus seven. This is because of the absent of phase shift, and the current influence of the three phases is accumulated.

With the respect of the variation of the magnetic flux density regarding the distance between cables and shaft, the point in the middle of the shaft is studied. The result is shown in Figure 4.15.

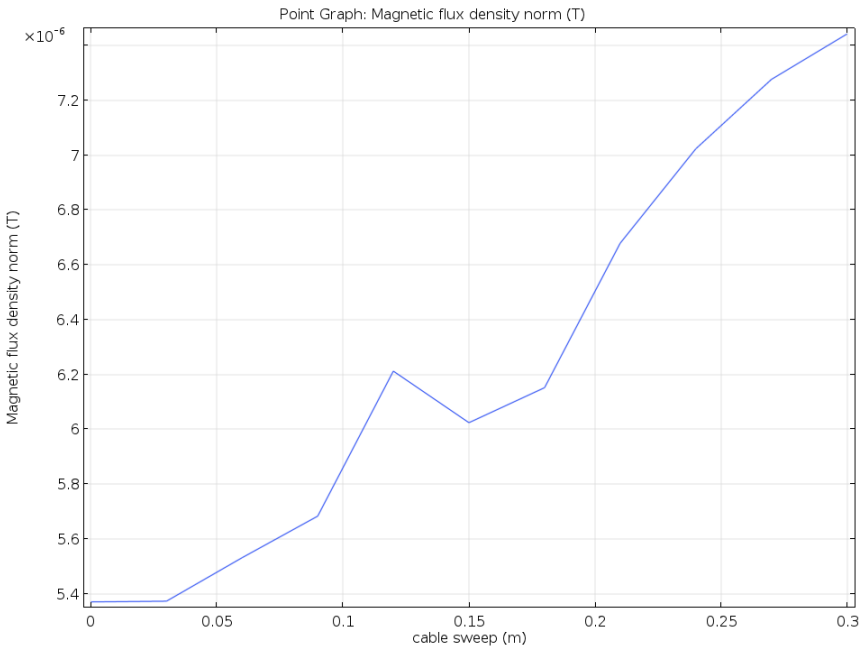

Figure 4.15: Magnetic flux density on the shaft with varied distance between cables and shaft

As it can be observed in Figure 4.15, the maximum flux density can be $7.4\mu T$. According to the induced voltage equation:

$$V = 4.44Nf\psi \tag{4.1}$$

where N is the number of turns, f is the current frequency(150Hz in this case since it is 3rd harmonics) and ψ is the total magnetic flux in a certain area. In another word, for each of one square meter near the shaft, the value of induced voltage on the shaft which can be detected is approximately $4.93mV$. Therefore, the next step is to investigate such voltage level can generate the same value as the measurement current or not.

4.2.2 Induced voltage determination

From the measurement, it can be observed that the current through the bearing is 10A. After performing a parametric sweep, the current voltage relationship was established which is shown in Figure 4.16.

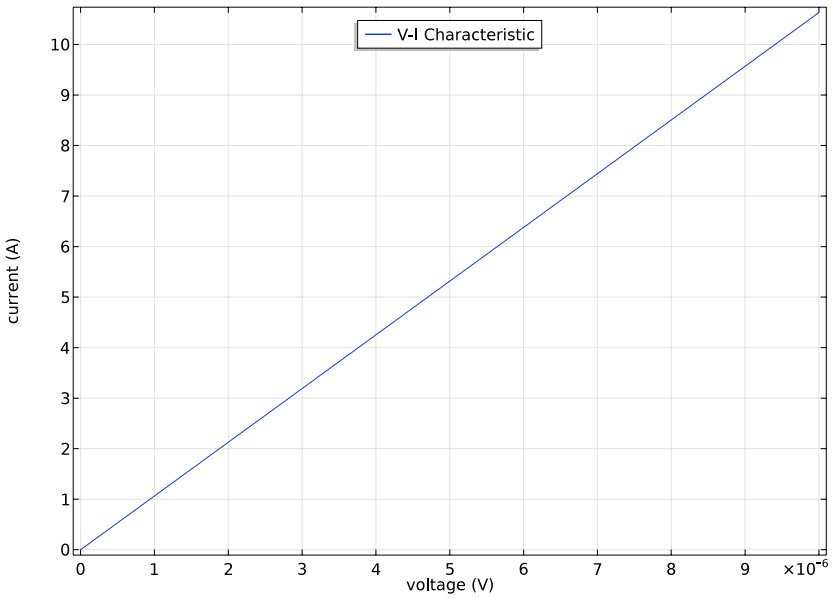

Figure 4.16: V-I characteristic on the foot of bearing

From Figure 4.16, it can be seen that it takes only $10\mu V$ to generate current of 10A magnitude. This means, only based on the simulation, the induced voltage on the shaft is possibly to generate the corresponding current in the measurement. However, in this simulation, the capacitance of the grease layer is totally ignored. If the capacitance of the grease layer has been taken into consideration, the induced voltage will increase up to milli scale. According to what is discussed above, it is still possible to generate such high current in the foot of the bearing

The last but not the least, the robustness of this simulation model need to be approved by investigating the real conductivity of all the components in simulation and the simulation based discharge mechanism in the lubricant.

5

Conclusion

5.1 Results of Current Study

In the measurement analysis of this project, it is mainly focused on FFT spectrum obtained from different measurements. As it has been mentioned in previous sections, there is some suspicious current on the shaft, bearings and especially grounding cables of converter and generator. As a summary of Section 4.1, a large amount of current, 74 A, with fundamental frequency 50 Hz flows in the converter grounding cable. Also, the current flowing in the shaft has the same fundamental frequency 50Hz; one can suspect that the excessive converter grounding current might lead some current to flow on the shaft. However, even though measurement which has been done on 15^{th} November 2017 shows that the dominant component in the shaft current analysis is the 50Hz fundamental component, another measurement on 11^{th} April 2017 does not correspond with each other. It is observed that 3^{rd} harmonics are dominant in the shaft currents, thus, for the further investigations the issue should be taken into account.

Besides those most distinguish results, by creating a open-loop conductor magnetic flux around the shaft has been tried to measure. Even if some induced voltage values with 50 Hz has been obtained in the loop, since its amplitude is too low, that would not be a cause of the current on the shaft. Moreover, because a current flows in the shaft, the induced voltage could be due to magnetic flux of the shaft current, that is, its own magnetic flux occurring naturally because of the current presence.

On the other hand, some currents flow through the generator grounding cable which includes 50 Hz grid frequency and 10 Hz generator frequency(turbine frequency). It is also a suspicious current which is not supposed to flow there. If more detailed analysis is needed, one should consider the current as well.

In respect of simulation in COMSOL. The proposal of induced voltage which is caused by the adjacent power cable over the shaft is modeled. First, the magnetic flux density near the shaft is obtained. Then, with the varying distance between the power cables and the shaft, the induced voltage is calculated. To investigate whether such voltage level can generate the corresponding current on the foot of the bearing or not, only lower voltage level is needed, compared with the maximum induced voltage, to generate such current in measurement.

Although the root cause is possibly the induced voltage, the robustness simulation model needs to be approved. On the one hand, the conductivity of each of the components might have deficits between reality and simulation which directly results in the inaccuracy of the model. On the other hand, regardless of the discharge mechanism in COMSOL, the lubricant is simply regarded as a resistor rather than a capacitor. Therefore, this proposal still needs to be proved in the future work.

5.2 Future Work

Even though one proposal has been proved that it might be the root cause of the current generated on the shaft based on simulation. However, there are still some possible causes to be proved. The shaft is directly attached to the bearing and the rotor of generator. Therefore, due to the parasitic inductance and the capacitance property of the bearing, it might generate RLC circuit where resonance can be possibly generated. Even though the resonance frequency is normally high and the frequency that is measured on the foot of the bearing is low, it is still possible due to the sampling frequency is relatively low. Another doubt is where does the current flow to on the blade side of the shaft. Due to the mismatch of the two measurements, more accurate measuring equipment should be adopted. The last but not the least, The converter grounding current is extremely large. therefore, the investigation of converter working principle should be conducted as well as the grounding system.

Bibliography

[1] *IEEE Code of Ethics*. [Online]. https://www.ieee.org/about/corporate/governance/p7-8.html. IEEE.

[2] Kristin Bruhn Sofia Lorensson Jennie Svensson. "Wind Power – A Renewable Energy Source in Time". In: *A comprehensive guide of wind power plants, its history, construction and impacts on the power grid* 17.3 (2009), pp. 40–60.

[3] Mats Leijon, Mikael Dahlgren, Lars Walfridsson, et al. "A recent development in the electrical insulation systems of generators and transformers". In: *IEEE Electrical Insulation Magazine* 17.3 (2001), pp. 10–15.

[4] M.Bongiorno. *power electronics solution to power system*. Chalmers university of technology. Nov. 2017.

[5] Mats Leijon, Mikael Dahlgren, Lars Walfridsson, et al. "A recent development in the electrical insulation systems of generators and transformers". In: *IEEE Electrical Insulation Magazine* 17.3 (2001), pp. 10–15.

[6] Yaqing Liu, Mihael Zitnik, and Rajeev Thottappillil. "An improved transmission-line model of grounding system". In: *IEEE Transactions on Electromagnetic Compatibility* 43.3 (2001), pp. 348–355.

[7] Seppo Hänninen and Matti Lehtonen. "Characteristics of earth faults in electrical distribution networks with high impedance earthing". In: *Electric Power Systems Research* 44.3 (1998), pp. 155–161.

[8] Siow Chun Lim, Chandima Gomes, and Mohd Zainal Abidin Ab Kadir. "Electrical earthing in troubled environment". In: *International Journal of Electrical Power & Energy Systems* 47 (2013), pp. 117–128.

[9] Donald W Zipse. "Earthing-grounding methods: a primer". In: *Petroleum and Chemical Industry Conference, 2001. IEEE Industry Applications Society 48th Annual*. IEEE. 2001, pp. 11–30.

[10] I Colominas, Javier Gómez-Calviño, F Navarrina, et al. "Computer analysis of earthing systems in horizontally or vertically layered soils". In: *Electric Power Systems Research* 59.3 (2001), pp. 149–156.

[11] FE Mentre and Leonid Grcev. "EMTP-based model for grounding system analysis". In: *IEEE Transactions on Power Delivery* 9.4 (1994), pp. 1838–1849.

[12] *Standard CWT technical notes*. [Online]. Available: http://www.pemuk.com/products /cwt-current-probe/cwt.aspx. PEM Power Electronic Measurements. Aug. 2002.

[13] *Materials Information System*. [Online]. Available: https://setis.ec.europa.eu/mis/technology/wind-energy. European Commission SETIS.

[14] *Nacelle*. [Online]. http://www.daviddarling.info/encyclopedia/N/AE$_n$*acelle.html*. The Encyclopedia of Alternative Energy and Sustainable Living.

[15] *Product Focus*. [Online]. http://www.pandct.com/Media/shownews.asp?ID=28652. Process and Control Today.

[16] *Big Glenn Project Schematic*. General Electric Company Wind Energy Company. Oct. 2011.

A

Appendix 1

A.1 FFT Matlab codes

Figure A.1 depicts Matlab codes utilized to obtain the single-sided amplitude spectrum of the signals in the results part.

```
%% calculating the single-sided amplitude spectrum



%Signal is the waveform the FFT function will be applied to it
%Tinterval is the time step of the data obtained from Picoscope
%Length is the length of the signal obtained from Picoscope

% recreating the time signal
Time = 0:Tinterval:(Length-1)*Tinterval;

% if it is intended to calculate the FFT between a specific time range the
% T_min and T_max must be specified before the code to limit the FFT to
% that interval
Time_range_FFT = find(Time>Time_min & Time<Time_max);
Time_FFT = 0:Tinterval:(length(Time_range_FFT)-1)*Tinterval;

% Shape the Signal waveform to perform FFT
Signal_FFT = Signal(Time_range_FFT)';

% the sampling frequency
Ts=Time_FFT(length(Time_FFT));

% the sampling period
Df=1/Ts;

% calculating the single-sided spectrum of the Signal
fftvect=fft(Signal_FFT)/length(Signal_FFT)*2;

% defining the frequency vector for the amplitude spectrum graph
freqvect=(0:length(Signal_FFT)-1)*Df;

%plotting the single-sided amplitude spectrum
loglog(freqvect([1:(length(Time_FFT)/2+1)]),abs(fftvect([1:(length(Time_FFT)/2+1)])));

```

Figure A.1: Matlab code to calculate the single-sided amplitude spectrum of a signal

A.2 The measurement data

Tables A.1 to A.6 depict the magnitudes of current harmonics measured at Big Glenn site on 15^{th} of November 2017. Similarly tables A.7 to A.10 represent the magnitudes of current harmonics measured at Big Glenn site on 11^{th} of April 2017.

Table A.1: The current harmonics magnitudes for the 1^{st} measurement performed at the Big Glenn site on November 15^{th} 2017.

Frequency [Hz]	10.9					50				Other			
Signals/Harmonic order	1^{st}	2^{nd}	3^{rd}	5^{th}	7^{th}	1^{st}	3^{rd}	5^{th}	7^{th}	4	17.7	85	107
Generator Cable	310.1	1.28	2.94	2.56	2.34	0	-	-	-	-	-	-	-
Converter Cable	-	-	-	-	-	154.3	1.22	2.32	2.29	-	-	-	-
Generator Ground	6.33	1.28	0.67	0.3	0.13	7.22	0.23	0.16	0.29	2.21	1.87	0.12	0.13
Converter Ground	0.65	0.25	0.16	-	-	75.19	1.43	1.14	1.71	0.38	0.29	-	-
Shaft current	0.67	-	0.36	-	-	5.46	-	0.1	0.11	-	-	0.15	0.14
Gen-side bearing current	9.04	0.81	6.01	1.51	1.26	0.44	-	-	-	-	1.15	0.5	0.5
Gen-to-bearing current	9.7	0.89	6.37	1.53	1.22	5.84	-	-	-	-	1.13	0.37	0.35

Table A.2: The current harmonics magnitudes for the 2^{nd} measurement performed at the Big Glenn site on November 15^{th} 2017.

Frequency [Hz]	10.9					50				Other			
Signals/Harmonic order	1^{st}	2^{nd}	3^{rd}	5^{th}	7^{th}	1^{st}	3^{rd}	5^{th}	7^{th}	4	17.7	85	107
Generator Cable	315	2.06	3	2.68	1.97	-	-	-	-	-	-	-	-
Converter Cable	-	-	-	-	-	153.6	1.2	2.6	2.3	-	-	-	-
Generator Ground	6.02	1.47	0.58	0.3	-	7.2	0.23	0.23	0.31	2.21	2.06	0.15	0.15
Converter Ground	0.56	0.27	-	-	-	74.85	1.4	1.44	1.7	0.41	0.31	0.22	-
Shaft current	0.66	-	0.4	0.22	-	5.4	-	0.1	0.13	-	0.18	0.19	0.16
Gen-side bearing current	9.33	1.03	6.04	1.51	0.97	0.44	-	-	-	-	1.34	0.48	0.53
Gen-to-bearing current	10	1.07	6.32	1.64	1.03	5.81	-	-	-	-	1.29	0.36	0.37

Table A.3: The current harmonics magnitudes for the 3^{rd} measurement performed at the Big Glenn site on November 15^{th} 2017.

Frequency [Hz]	10.8					50				Other			
Signals/Harmonic order	1^{st}	2^{nd}	3^{rd}	5^{th}	7^{th}	1^{st}	3^{rd}	5^{th}	7^{th}	4	17.6	84.4	105.8
Generator Cable	330.2	1.32	3.85	2.86	3	-	-	-	-	-	-	-	-
Converter Cable	-	-	-	-	-	108.1	1.03	2.86	1.89	-	-	-	-
Generator Ground	8.2	2.06	1.1	-	-	5.16	0.26	0.17	0.3	1.75	1.99	0.23	0.2
Converter Ground	0.86	0.4	-	-	-	52.72	1.31	1.46	1.43	0.32	0.36	-	-
Shaft current	0.72	-	0.54	-	-	3.84	-	0.1	0.1	-	-	0.25	0.19
Gen-side bearing current	8.74	1.36	6.57	1.57	1.3	0.49	-	-	-	-	1.25	0.87	0.69
Gen-to-bearing current	9.46	1.42	7.1	1.76	1.38	4.21	-	-	-	-	1.21	0.62	0.52

Table A.4: The current harmonics magnitudes for the 4^{th} measurement performed at the Big Glenn site on November 15^{th} 2017.

Frequency [Hz]	11					50				Other			
Signals/Harmonic order	1^{st}	2^{nd}	3^{rd}	5^{th}	7^{th}	1^{st}	3^{rd}	5^{th}	7^{th}	4	18	86	108
Generator Cable	272	0.83	2.48	2.4	1.85	-	-	-	-	-	-	-	-
Converter Cable	-	-	-	-	-	107.2	1.3	2.9	1.74	-	-	-	-
Generator Ground	4.91	1.5	0.66	0.35	0.16	5	0.25	0.2	0.21	1.61	1.88	0.21	0.13
Converter Ground	0.56	0.31	-	-	-	52.19	1.44	1.49	1.3	0.25	0.28	-	-
Shaft current	0.66	-	0.5	0.2	-	3.78	-	0.12	0.1	-	-	0.23	0.25
Gen-side bearing current	8.57	1.1	5.2	1.34	0.89	0.46	-	-	-	-	1.17	0.73	0.79
Gen-to-bearing current	9.23	1.1	5.7	1.53	1	4.15	-	-	-	-	1.23	0.56	0.55

Table A.5: The current harmonics magnitudes for the 5^{th} measurement performed at the Big Glenn site on November 15^{th} 2017.

Frequency [Hz]	10.8					50				Other			
Signals/Harmonic order	1^{st}	2^{nd}	3^{rd}	5^{th}	7^{th}	1^{st}	3^{rd}	5^{th}	7^{th}	4	17.7	85	107
Generator Cable	230	1.35	2.76	3.39	3.03	-	-	-	-	-	-	-	-
Converter Cable	-	-	-	-	-	136.1	1.58	2.57	1.98	-	-	-	-
Generator Ground	5.32	2.04	0.84	0.38	-	6.39	0.34	0.22	0.24	2.21	2.47	0.24	0.2
Converter Ground	0.51	0.36	-	-	0.59	66.29	1.84	1.38	1.47	0.38	0.39	-	-
Shaft current	0.54	-	0.48	-	0.25	4.84	-	0.1	0.11	-	-	0.34	0.28
Gen-side bearing current	6.5	1.38	5.89	1.79	1.36	0.5	-	-	-	-	1.59	1.06	0.88
Gen-to-bearing current	7.03	1.49	6.35	1.95	1.47	5.2	-	-	-	-	1.54	0.72	0.61

Table A.6: The current harmonics magnitudes for the 6^{th} measurement performed at the Big Glenn site on November 15^{th} 2017.

Frequency [Hz]	10.8					50				Other			
Signals/Harmonic order	1^{st}	2^{nd}	3^{rd}	5^{th}	7^{th}	1^{st}	3^{rd}	5^{th}	7^{th}	4	17.6	84.2	105.6
Generator Cable	236	1	3.1	2	1.78	-	-	-	-	-	-	-	-
Converter Cable	-	-	-	-	-	153	1.14	3.1	2	-	-	-	-
Generator Ground	3.9	1.24	0.6	0.24	-	7.16	0.23	0.22	0.25	1.47	1.58	-	0.14
Converter Ground	0.55	0.21	-	-	-	74.6	13	1.6	1.5	0.26	0.29	-	-
Shaft current	0.66	-	0.62	0.25	-	5.54		0.1	0.1	-	-	0.27	0.25
Gen-side bearing current	6.51	0.81	5.27	1.02	0.77	0.5	-	-	-	-	0.95	0.61	0.61
Gen-to-bearing current	7.17	087	5.89	1.23	0.85	5.94	-	-	-	-	1.04	0.38	0.36

Table A.7: The current harmonics magnitudes for the 1^{st} measurement (uppstart 8<t<10) performed at the Big Glenn site on April 11^{th} 2017.

Frequency [Hz]	10.75					50
Signals/Harmonic order	1^{st}	2^{nd}	3^{rd}	5^{th}	7^{th}	1^{st}
Generator Cable	22.2	1.63	0.39	0.59	0.48	-
Hub foot bearing current	0.46	-	1.1	0.31	-	-
shaft current toward hub	*	-	-	-	-	0.02
Shaft current	0.46	0.1	1.08	0.31	-	-
Gen-side bearing current	1.35	0.5	3.2	0.97	0.46	-
Gen-to-bearing current	0.89	0.38	2.1	0.67	0.36	-

Table A.8: The current harmonics magnitudes for the 2^{nd} measurement (uppstart 16<t<18) performed at the Big Glenn site on April 11^{th} 2017.

Frequency [Hz]	10.75					50
Signals/Harmonic order	1^{st}	2^{nd}	3^{rd}	5^{th}	7^{th}	1^{st}
Generator Cable	246	-	3.85	2.48	2.3	-
Hub foot bearing current	3.72	0.73	6.3	1.4	-	1.34
shaft current toward hub	0.01	-	-	-	-	0.47
Shaft current	3.71	0.73	6.3	1.4	0.55	1.74
Gen-side bearing current	9.07	1.74	14.16	2.9	1.6	2.35
Gen-to-bearing current	5.36	1	7.9	1.8	1.02	-

Table A.9: The current harmonics magnitudes for the 3^{rd} measurement (drift2-C10V, 8<t<12) performed at the Big Glenn site on April 11^{th} 2017.

Frequency [Hz]	10.75					50				Other	
Signals/Harmonic order	1^{st}	2^{nd}	3^{rd}	5^{th}	7^{th}	1^{st}	3^{rd}	5^{th}	7^{th}	85	106
Generator Cable	292	3.22	3.5	3.03	4.32	-	-	-	-	-	-
Hub foot bearing current	9.74	1	13.3	2.1	1.37	2.71	-	-	-	1.05	0.64
shaft current toward hub	*	-	0.02	-	*	0.83	*	*	*	-	-
Shaft current	9.73	1.05	13.3	2.1	1.4	3.4	-	-	-	1.05	0.64
Gen-side bearing current	24.4	2.4	30.72	5.6	3.8	3.96	-	-	-	-	-
Gen-to-bearing current	14.68	1.47	17.5	3.47	2.46	-	-	-	-	-	-

Table A.10: The current harmonics magnitudes for the 4^{th} measurement (drift3-C10V, 14<t<18) performed at the Big Glenn site on April 11^{th} 2017.

Frequency [Hz]	10.75					50				Other	
Signals/Harmonic order	1^{st}	2^{nd}	3^{rd}	5^{th}	7^{th}	1^{st}	3^{rd}	5^{th}	7^{th}	85	106
Generator Cable	292	2.4	3.47	2.51	2.4	-	-	-	-	-	-
Hub foot bearing current	9.1	1.15	11.6	1.5	1.1	2.33	-	-	-	0.68	0.68
shaft current toward hub	0.03	*	*	-	-	0.69	*	*	*	-	-
Shaft current	9.12	1.16	11.58	1.55	1.1	2.01		-	-	0.7	0.68
Gen-side bearing current	5.36	0.56	4.5	1.7	0.9	2.14	-	-	-	0.96	0.9
Gen-to-bearing current	14.18	1.5	16.07	2.93	1.67	-	-	-	-	0.3	0.23

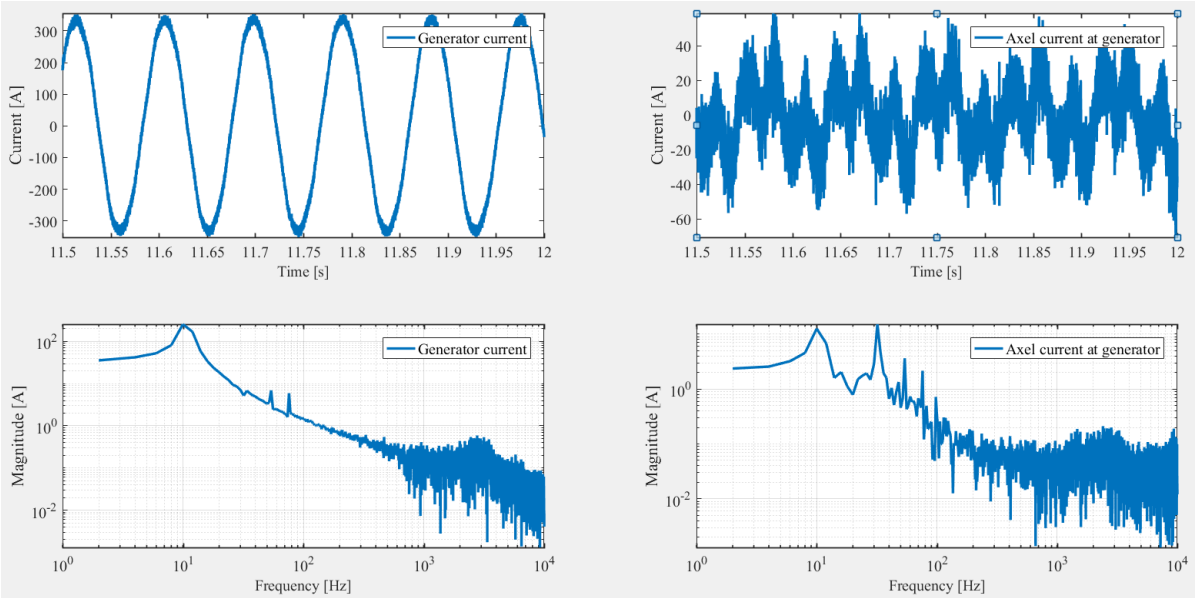

Figure A.2: Generator current and axle-current-at-generator waveforms and single-sided amplitude spectrum for the 3^{rd} measurement (drift2-C10V, 8<t<12) performed at the Big Glenn site on April 11^{th} 2017.

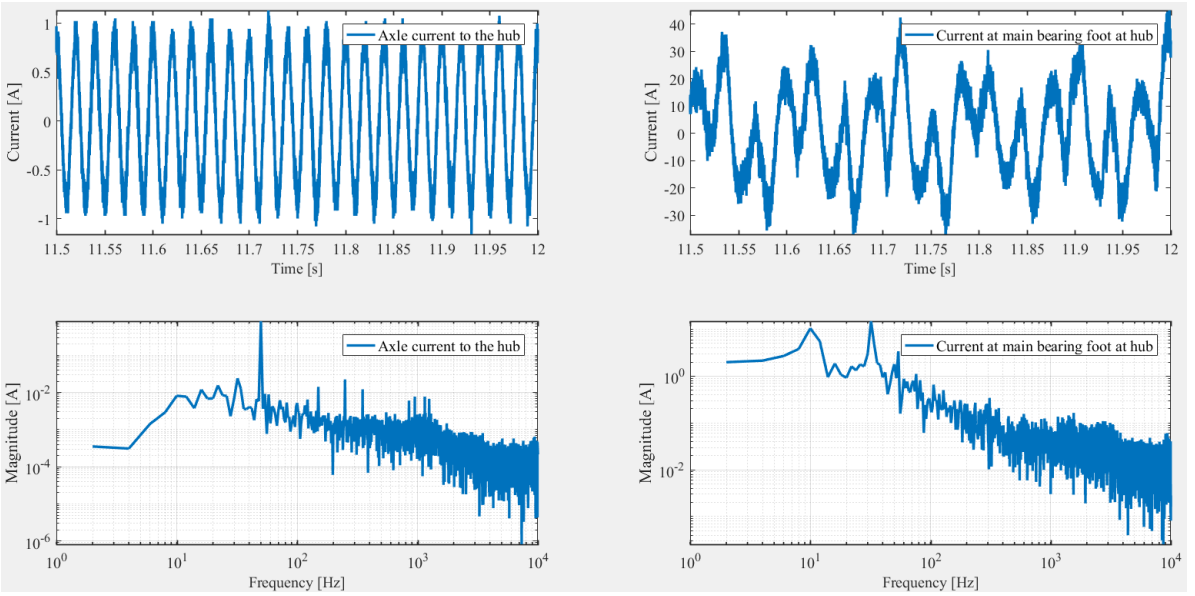

Figure A.3: Axle-current-to-the-hub and current-at-the-main-bearing-foot-at-the-hub waveforms and single-sided amplitude spectrum for the 3^{rd} measurement (drift2-C10V, 8<t<12) performed at the Big Glenn site on April 11^{th} 2017.

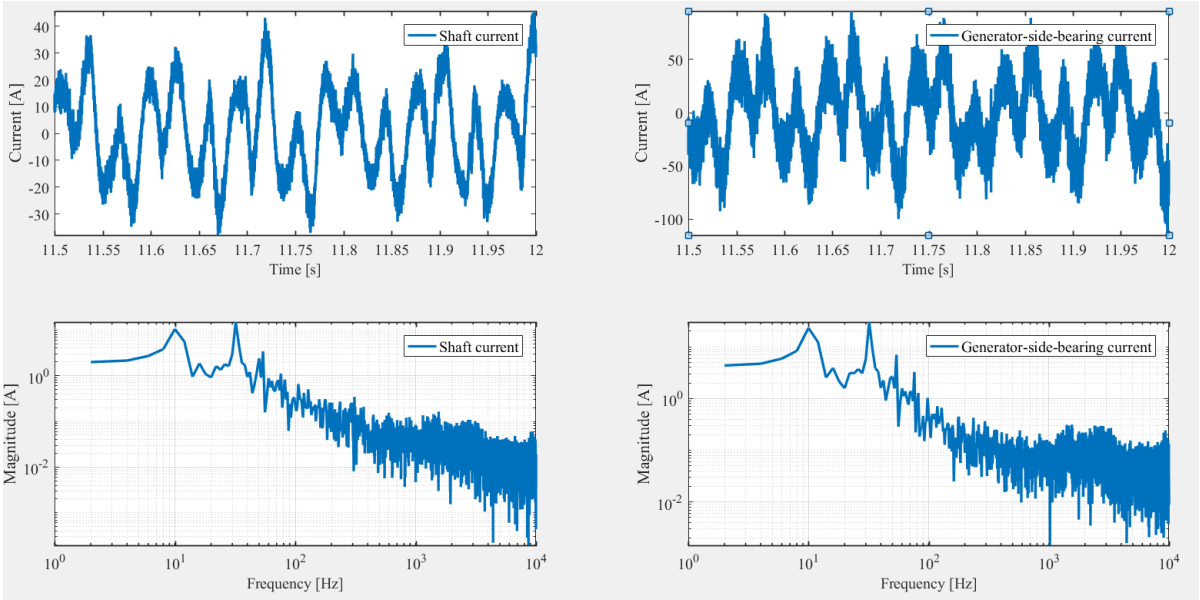

Figure A.4: (derived with applying KCL)Shaft current and generator-side-bearing current waveforms and single-sided amplitude spectrum for the 3^{rd} measurement (drift2-C10V, 8<t<12) performed at the Big Glenn site on April 11^{th} 2017.

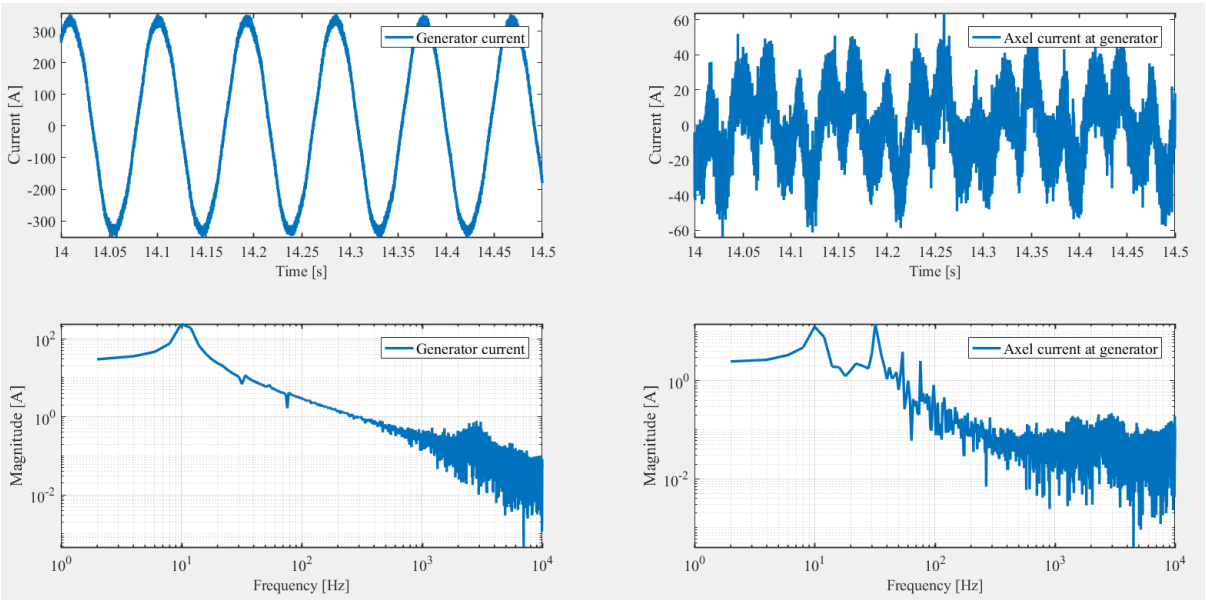

Figure A.5: Generator current and axle-current-at-generator waveforms and single-sided amplitude spectrum for the 4^{th} measurement (drift3-C10V, 14<t<18) performed at the Big Glenn site on April 11^{th} 2017.

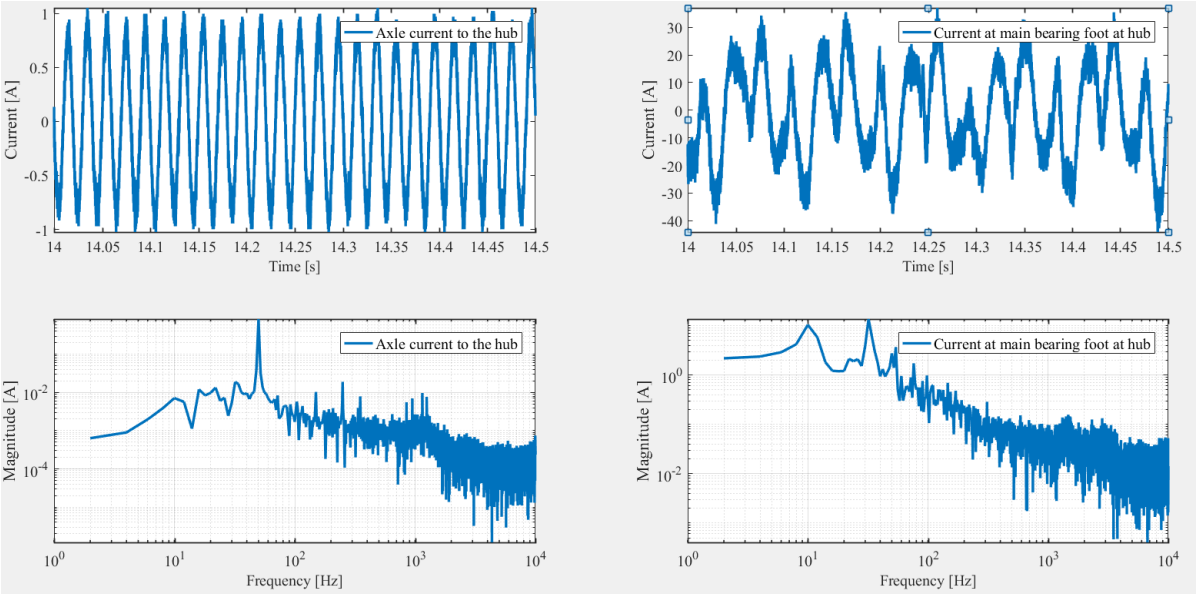

Figure A.6: Axle-current-to-the-hub and current-at-the-main-bearing-foot-at-the-hub waveforms and single-sided amplitude spectrum for the 4^{th} measurement (drift3-C10V, 14<t<18) performed at the Big Glenn site on April 11^{th} 2017.

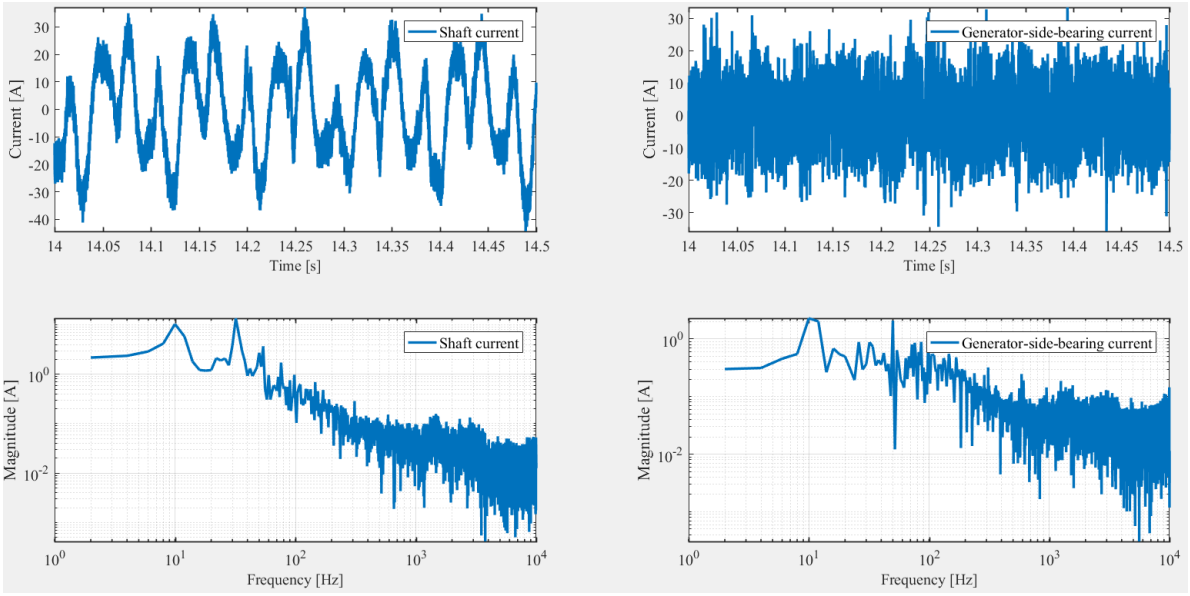

Figure A.7: (derived with applying KCL)Shaft current and generator-side-bearing current waveforms and single-sided amplitude spectrum for the 4^{th} measurement (drift3-C10V, 14<t<18) performed at the Big Glenn site on April 11^{th} 2017.